

Exploration of a simple model for ice ages

**A. C. Fowler, R. E. M. Rickaby &
E. W. Wolff**

**GEM - International Journal on
Geomathematics**

ISSN 1869-2672

Int J Geomath
DOI 10.1007/s13137-012-0040-7



 Springer

Your article is protected by copyright and all rights are held exclusively by Springer-Verlag. This e-offprint is for personal use only and shall not be self-archived in electronic repositories. If you wish to self-archive your work, please use the accepted author's version for posting to your own website or your institution's repository. You may further deposit the accepted author's version on a funder's repository at a funder's request, provided it is not made publicly available until 12 months after publication.

Exploration of a simple model for ice ages

A. C. Fowler · R. E. M. Rickaby · E. W. Wolff

Received: 18 April 2012 / Accepted: 23 June 2012
© Springer-Verlag 2012

Abstract We argue that, while Milanković variations in solar radiation undoubtedly have a major influence on the timing of the Quaternary ice ages, they are partly incidental to their underlying causes. Based on observations of the significance of CO₂, we propose a conceptually simple (but complicated in detail) energy balance type model which has the ability to explain the underlying oscillatory nature of ice ages. We are led to develop a model which combines ice sheet growth and atmospheric energy balance with ocean carbon balance. In order to provide results which mimic the basic features of the observations, we develop novel hypotheses as follows. The succession of the most recent ice ages can be explained as being due to an oscillation due to the interaction of the growing northern hemisphere ice sheets and proglacial lakes which form as they migrate south. The CO₂ signal which faithfully follows the proxy temperature signal can then be explained as being due to a combination of thermally activated ocean biomass production, which enables the rapid CO₂ rise at glacial terminations, and enhanced glacial carbonate weathering through the exposure of continental shelves, which enables CO₂ to passively follow the subsequent glacial cooling cycle. Milanković variations provide for modulations of the amplitude and periods of the resulting signals.

A. C. Fowler (✉)
MACSI, University of Limerick, Limerick, Republic of Ireland
e-mail: andrew.fowler@ul.ie

A. C. Fowler
OCIAM, University of Oxford, Oxford, UK

R. E. M. Rickaby
Department of Earth Sciences, University of Oxford, Oxford, UK

E. W. Wolff
British Antarctic Survey, High Cross, Madingley Road, Cambridge, UK

Keywords Ice ages · Milanković · Energy balance model · Proglacial lakes · Carbonate weathering

Mathematics Subject Classification 86A40

Contents

1	A critique of the Milanković theory of ice ages
2	Background and outline
3	A simple model of ocean carbon
3.1	The carbon cycle
3.2	The ocean-atmosphere model
3.3	An application to post-Eocene cooling
3.4	An application to global warming
4	Climate and ice sheet models
4.1	A simple climate model
4.2	Nucleation and growth of ice sheets
5	Combined ice and carbon model
5.1	The full dimensionless model
5.2	The onset of ice ages
6	Proglacial lake formation
6.1	Glacial retreat
6.2	The proglacial lake equation
7	Rapid CO ₂ rise
7.1	Continental shelf exposure
7.2	River chemistry
7.3	Bioproduction
8	Numerical results
8.1	Numerical method
8.2	Enhanced carbonate weathering
8.3	Milanković variations
9	Discussion
10	Conclusions

1 A critique of the Milanković theory of ice ages

At any timescale beyond the seasonal cycle, the strongest signal in Pleistocene climate at the global scale is the quasi-regular alternation between glacial periods (ice ages) and interglacials. The idea that this pattern was driven by variations in the received solar radiation due to variations in the Earth's orbit was advanced by [Croll \(1864, 1875\)](#). It was then championed by [Milanković \(1941\)](#), with whose name the theory is now largely associated. Milanković was able to calculate the solar radiation received at different latitudes and seasons based on the astronomical parameters (with what in retrospect can be seen as reasonable accuracy back to about 300 ka before present, [Berger 1988](#)). He then adopted the idea that the main determinant of ice sheet growth was the insolation (incoming solar radiation) received at high latitudes in the summer half year. These two advances allowed him to compare theory with the then-prevailing knowledge of the timing of ice advances in the European Alps, with what appeared to be success.

Improved knowledge of the timing of glaciation around the world, including the more integrated picture found in marine sediment cores, showed that his initial proc-

lamation of success was premature. However, the theory experienced a renaissance with the revelation by [Hays et al. \(1976\)](#) that the climate of the last half million years, as recorded in oxygen isotopes in marine sediments, shares its spectral peaks at 100, 41, 23 and 19 ka with those of the Earth's orbital variations associated with eccentricity, obliquity and precession. This is often seen as a verification of what has become known as Milanković theory. However, in reality it appears to be a much more limited confirmation that the astronomical cycles play a role in pacing the observed climate variations: the paper by [Hays et al. \(1976\)](#) specifically used the word “pacemaker” in its title, and explicitly pointed out that the dominance of the 100 ka cycle in their records required a nonlinear relationship between forcing and climate at this period. There are a number of problems with the theory as originally formulated by Milanković, and with many of its looser variants that may more generally be termed as astronomical theory, and we discuss these below.

Most obviously, it is clear that other major climatic effects must have been operative, in order that the Pleistocene ice ages begin at all. The late Pliocene was exceptionally warm, despite having the same solar variations occurring. Some other, presumably internal, factor must have changed, such that the same external forcing led to repetitive glaciations in one case, and to a persistent lack of northern hemisphere glaciation in the other. Similarly, the dominant period of Earth's climate changed from 40 ka in the period before about 1 Ma ago to 100 ka in the last 500 ka or more, again despite rather similar astronomical forcing. More particularly, while this dominant ice age period of 100 ka over the last 500 ka is associated with the frequency of eccentricity variations, the amplitude of the forcing is tiny. If ice ages are fundamentally due to the Milanković forcing, then some resonant response to this forcing seems necessary to provide the ice sheet response which is observed. However, if this is true, then it already tells us that the internal dynamics of the Earth's climate has a large part to play in the mechanism of ice age occurrence. As indicated by [Le Treut and Ghil \(1983\)](#) and [Tziperman et al. \(2006\)](#), this essentially suggests that the solar radiation variation may provide a nonlinear tuning mechanism for what is essentially an internal oscillation.

The situation does not improve in the earlier part of the Pleistocene: the dominant forcing of the solar radiation at a given latitude is associated with the precession of the equinoxes, with a period around 20 ka, but this seems inconsistent with the early Pleistocene periodicity of 40 ka; differing mechanisms have been put forward to account for this discrepancy ([Huybers 2006](#); [Raymo et al. 2006](#)); the latter of these proposes that both the Antarctic Ice Sheet and the Northern Hemisphere ice sheets may respond at precessional frequencies, but that their effects cancel out in the observational record.

A more direct critique of Milanković theory comes from an assessment of its performance against data in the time domain. For example, efforts have been made to correlate the time series of the 65° N radiation variation with the timings of ice age terminations ([Kawamura et al. 2007](#); [Cheng et al. 2009](#)). However, [Parrenin and Paillard \(2003\)](#) draw attention to the difficulties of the theory, and in particular point out inconsistencies with the times of sea level rise and times of maximum solar insolation. We restrict ourselves to the last four glacial cycles, and use the insolation curve of mid-summer (June 21) insolation at 65° north, a popular and close relation to the summer half-year insolation curves calculated by Milanković. Then (Fig. 1) it is possible to find rises in insolation that match the major warmings seen in the record of benthic

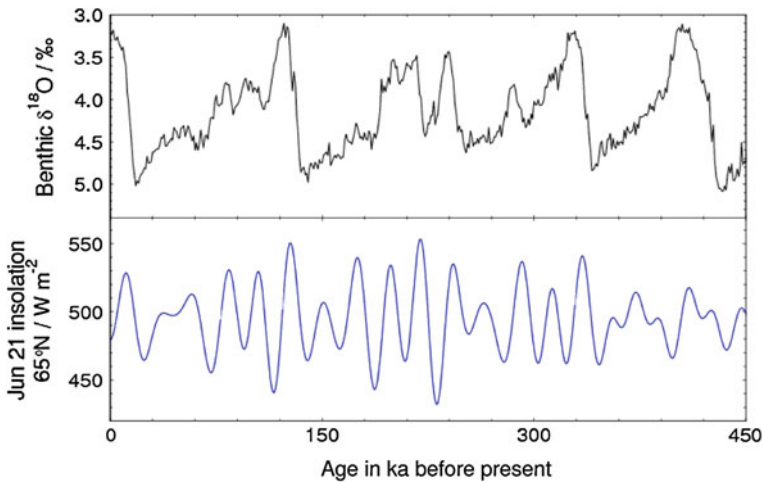


Fig. 1 Benthic oxygen isotopes (Lisiecki and Raymo 2005) and an insolation curve for 65° north on June 21st (Laskar et al. 2004) for the last 450 ka

oxygen isotopes (a modern version of the curve used by Hays et al. 1976). But there are numerous other rises in insolation, as large or larger than these, which caused no such change. Milanković theory, without substantial elaboration, simply has no predictive power.

The basic implicit model of the Milanković theory, never explicitly stated, is that the climate responds in a linear fashion to the solar radiation forcing. If it does not, then the spectral resemblance has no meaning. But if the response is linear, how can we explain the nonlinear form of the basic ice age cycle, with slow decline of the temperature, followed by relatively rapid rise at ice age termination? This in itself tells us that, at the least, the climate responds nonlinearly to the forcing.

A final issue is that it is difficult to sustain the Milanković notion that it is summer solar insolation at 65° N which drives the ice age climate. Wolff et al. (2009) are among a number of authors who point out that the sequence of events in the last and previous terminations was that the southern hemisphere warmed considerably before either major changes in high latitude northern climate, or a very significant rise in sea level (and loss of ice volume), kicked in; along with other authors, they also suggest that the millennial scale variability in climate, which is pervasive in the last glacial period, plays a central role in glacial terminations, an aspect that is not even considered in Milanković theory.

Hysteresis

Almost entirely absent in discussions of the Milanković forcings are why they cause what appears to be a relaxational oscillation between cold and warm states. The seminal papers of Budyko (1969) and Sellers (1969) are key in this context, because they propose that the transition to an ice age climate occurs through an imposed forcing due to solar radiation. Through the concept of ice-albedo feedback, they show that a

hysteretic switch between glacial and inter-glacial periods can be explained due to the inter-dependence of ice cover and atmospheric temperature. However, this explanation of ice ages has a conceptual difficulty. Typically, such hysteretic switches involve sudden jumps between cold and warm states, and vice versa. There is a long cold state followed by a long warm state. Evidently, this is not the case in ice ages. It is actually quite difficult to conceive of a way in which oscillations can occur, where there is a slow cooling followed by a sudden warming. Essentially, it seems we would need (at least) two slow variables and one fast one, and this already suggests a more complicated picture than the *Budyko-Sellers* one. An alternative is an autocatalytic reaction model which can provide explanations of spiking in glycolysis, for example *Goldbeter (1996)*.

A simpler alternative allows for the asymmetry in the growth of ice sheets and their decay. The growth of an ice sheet towards equilibrium occurs on a time scale which is controlled by the slow viscous flow of the ice, typical time scales for which lie in the range 10^4 – 10^5 years. On the other hand, wastage of ice sheets can be a much faster process, because the removal of meltwater is essentially instantaneous, and the formation of pro-glacial lakes only enhances the wastage by enabling calving.

Carbon

One of the striking results that emerged from the Antarctic ice core analysis (*Petit et al. 1999*) was the essential identity of the carbon dioxide signal with the proxy temperature signal (Fig. 2). There is seemingly an important lesson to be learned from this. It is that carbon plays a fundamental rôle in the ice age oscillations, and may indeed be

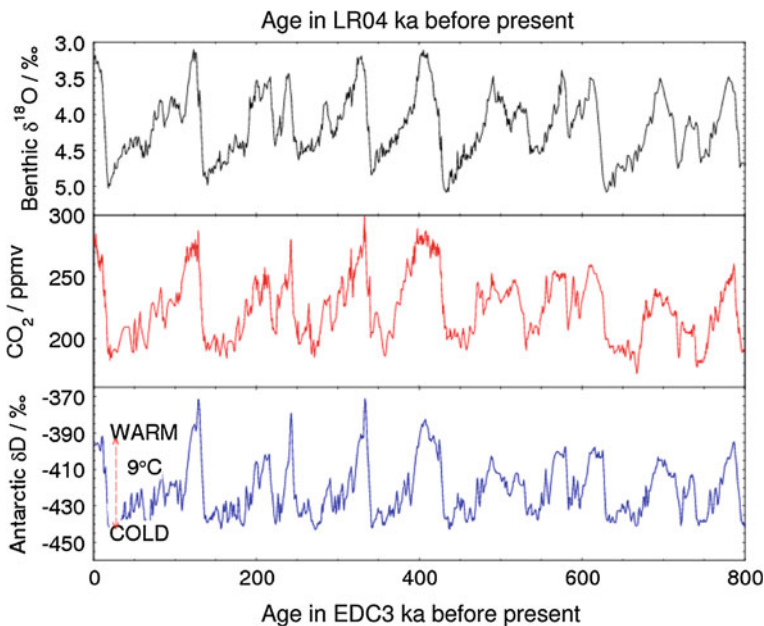


Fig. 2 Proxy temperature measurements from deep sea sediments (*top*), Antarctic ice core (*bottom*), and the CO_2 variation derived from the same Antarctic ice core

the driver for ice ages. This is consistent with a prevailing viewpoint that on a longer time scale, it is the CO_2 in the atmosphere which controls global temperatures.

At first sight, it seems reasonable that CO_2 and temperature T would follow each other closely. After all, we expect global atmospheric temperature to be a function of CO_2 partial pressure p_{CO_2} because of the greenhouse effect. But T depends on other quantities also, in particular radiation balance implies

$$T = T(p_{\text{CO}_2}, a), \quad (1.1)$$

where a is the planetary albedo. One might also suppose that T depends on the primary greenhouse gas H_2O , but the water vapour in the atmosphere and the consequent cloudiness itself depend directly on temperature, so that there is no independent effect.

If, for example, ice age oscillations occurred because of the insolation-driven switches between the different Budyko-Sellers states, there would be no need for CO_2 to vary at all: the oscillations would occur because of the dependence of albedo on ice cover and thus temperature. This is something of an oversimplification because of the 'solubility pump', which arises due to the fact that the solubility of CO_2 decreases as temperature increases. Thus during an ice age, the increased solubility drives the atmospheric CO_2 lower. However, it is not generally considered that this variation is sufficient to explain the observed variation of CO_2 , which would need a change of global average temperature of some 15°K , about two or three times that which is thought to have occurred. In fact this effect is offset by the fact that solubility decreases with increasing salinity (which occurs because of sea level lowering), which makes its importance even less. The fact that T and CO_2 are essentially identical therefore tells us directly that the oscillations in carbon are not directly a consequence of the oscillations in temperature, and must therefore form an integral constituent of the oscillation mechanism. Since there is no direct effect of solar radiation variations on CO_2 , we see that these provide a modulative, but not causative, effect.

In this paper, we suggest a simple model which might provide a basic mechanism for self-sustained oscillations with a 100 ka timescale. Such suggestions are not new; for example, [Toggweiler \(2008\)](#) has suggested a dominant role in the 100 ka cycle for oceanic carbon, and the model which we suggest incorporates carbon as a fundamental controlling variable. A similar approach, both in ethos and in some of the detail, can be found in the papers by [Saltzman and Maasch \(1988\)](#), [Maasch and Saltzman \(1990\)](#), and [Saltzman and Maasch \(1991\)](#). In these papers, the authors follow the same philosophical line as that advanced here, namely that the principal driver of the ice age oscillations is to be sought in a model which portrays self-sustained oscillations, and that these are modulated by the Milanković variations. The essential difference between Saltzman and Maasch's work and that presented here is that their eventual portrayal of the dynamics of the Earth's climate system does not involve the details of the constituent processes in a specific way. A similar approach has been taken by Ghil and co-workers ([Källén et al. 1979](#); [Ghil and Le Treut 1981](#); [Le Treut and Ghil 1983](#)), although their models do not consider the role of carbon.

The last and most thorough exposition of Saltzman's theory is in his voluminous book on the subject ([Saltzman 2002](#)). There is very little in the present paper which is not covered, often in detail, in Saltzman's work, and it is worth emphasising the

slightly different flavour which we import. An example will suffice. In his chapter 10, he deals in detail with the carbon cycle, mirroring our presentation below. For example, our buffering relation (3.37) below transiently connects to Saltzman's equation (10.9). Even our putatively novel introductions of thermally activated biomass and phosphate limited growth are included (on page 186 and page 189, respectively). Having discussed these and a number of other ingredients, Saltzman steps back. On page 191, he assumes (in (10.27) and then (10.28)) an essentially arbitrary functional form for the air-sea CO₂ exchange flux. On the following page, he states that it is 'beyond our capabilities' to properly constrain these terms, but suggests that 'it is of great value to pursue the development of more detailed models'. It is our conceit that this is the intent of the present work.

2 Background and outline

The present paper is so long, and its logic so involved, that we here outline our thesis, our goals, and the logic that has driven the paper to its conclusion. In addition, we preface each of the following Sects. 3 to 8 with preambular summaries.

Our thesis is based on the data presented in Figs. 1 and 2. We take the first to show that the Milanković variation of solar insolation provides a modulative, but not causative, effect on ice age occurrence, at least over the last million years. Ice age periodicity is thus the result of an internal oscillation, and the second figure suggests that, since atmospheric carbon mirrors the ice age temperature variation, carbon may act as the driver for this periodicity.

We thus begin our campaign by constructing a model for the variation of atmospheric carbon dioxide. This is done in Sect. 3. In keeping with our efforts to devise the simplest possible theory, our model is a box model. Its essential constituent variable is the atmospheric CO₂ partial pressure, which is produced by volcanic outgassing (and more recently by human agency), and removed by aerial dissolution in rain droplets, precipitation, rock weathering via dissolution, and runoff to the ocean. In addition, CO₂ dissolves directly in the ocean, and so its atmospheric partial pressure is tied to that in the ocean, which is however buffered by the presence of carbonate and bicarbonate ions. In turn, the concentrations of these are coupled to ocean calcium concentrations, because oceanic plankton such as coccolithophores use calcium and carbonate to form their shells. The uptake rate of carbonate thus involves the ocean biomass, and in addition the concentration of whatever is rate-limiting for biomass growth, which we take to be phosphorus. Our 'simple' model for carbon thus leads to a complicated nonlinear model involving eight separate chemical reactants (hydrogen ion in addition to those alluded to above).

Despite its complexity, we are able to describe analytically the behaviour of the solutions. The oceanic carbon system model is stable. In addition, we use the model to provide an explanation of Cenozoic planetary cooling, and to illustrate the possibly dire consequences of anthropogenic global warming beyond the century time scale which is the focus of most climate prediction models.

Section 4 adds two ingredients to the carbon system. Planetary temperature is determined by a global energy balance which depends on the greenhouse effect of CO₂, and

the reflected short wave radiation due to varying ice cover (and thus albedo). This raises the necessity to provide an ice sheet growth model, and the simplest such model representing growth of land-terminating ice sheets is presented, providing another ordinary differential equation for the ice sheet extent, which has a hysteretic but non-oscillatory behaviour as the planetary temperature varies.

The carbon, temperature and ice models are all in practice interconnected, and thus in Sect. 5 we combine them. This allows us first to provide a quantitative explanation for the cooling of the planet since the Eocene, and the successive growth of the Antarctic, Greenland and Laurentide ice sheets; but still there are no oscillations. Milanković variations can drive oscillations, but they are sinusoidal and of too short period.

The following Sect. 6 then attacks the specific question of how to produce self-sustaining 100 ka oscillations, and in addition rapid glacial terminations. The key to our investigation is the observation that glacial terminations occur in 10 ka. There needs to be something explicit in the model which allows ice sheet wastage to be more rapid than accumulation. We hypothesise that the mechanism is due to the formation of proglacial lakes, which allow rapid wastage through iceberg calving and melting. As it turns out, this idea is not all new, being considered by Pollard (1982), with a similar purpose. However, our approach is somewhat different. If proglacial lakes provide a mechanism to allow rapid melting, then it is necessary to include in the model an explicit evolution equation for the proglacial lake volume, and this is done. Surprisingly, and without hunting, the coupled ice sheet/proglacial lake model produces self-sustained oscillations, of the correct period and sawtooth form.

At this stage, we have been led far from our initial hypothesis that carbon drives ice age oscillations: carbon is irrelevant! Of course, because carbon is coupled to the ice sheet model, the ice sheet/proglacial lake oscillations do cause oscillations in carbon; but, mainly because the response time is slow (being controlled by the oceans), these oscillations are most unlike the observations. Thus, in Sect. 7, we undertake a detective chase for mechanisms which might cause the observed carbon behaviour. Because we have retained an analytic understanding of the behaviour of the model, we are able in effect to deduce what mechanism must operate to produce the observations.

One possibility, ocean salinity alteration due to sea level lowering, is examined but found wanting. A second mechanism involves the differing weathering rates during ice ages, which might have allowed slight changes in ocean salinity with consequent significant change in carbon, but this also does not work. Next, we realise that in order to find rapid CO₂ increase during termination, a rapid response time scale is necessary, and this can be provided by the ocean phosphate time scale. This leads us to propose that as the temperature rises, ocean biomass responds rapidly, leading to a rapid drawdown of oceanic carbonate, and consequent rise in atmospheric CO₂.

Having finally found the rapid carbon rise mechanism, we proceed in Sect. 8 to provide numerical solutions. Our aim is to reproduce eight specific features of the solutions: rapid terminations, rapid CO₂ rise, correct CO₂ jump, maximum ice extent of ~4,000 km, present day ocean carbonate and bicarbonate levels, slow glacial CO₂ decline, temperature fluctuations of ~5 K, and 100 ka periodicity. Immediately we find that CO₂ fails to follow the ice sheet extent down during interglacials, and we resort to a further enhancement, again based on an analytic understanding of the model. This assumes enhanced carbonate weathering during ice ages, due presumably to the

exposure of continental shelves; this is also a known hypothesis—the coral reef hypothesis (Berger 1982), and our analysis indicates that even a mild increase is able to force the CO_2 to follow the temperature down during glacial periods. With this on board, a non-exhaustive search using mild adjustment of twelve parameters is able to satisfy our eight constraints.

Finally, we add a representation of Milanković variations to the model. As we might now expect, the oscillations become somewhat irregular, although not as much as the data indicates, which may be due in the latter to the occurrence of Dansgaard–Oeschger events. The final discussion and conclusions draw together the outcomes of the study.

3 A simple model of ocean carbon

Preamble

In this section, we begin the task of constructing the simplest model which will eventually provide a possible explanation of the rough form of the Pleistocene ice age oscillations. We assume that CO_2 is a fundamental variable, and thus our model will essentially be a CO_2 balance model, as suggested by Toggweiler (2008). A number of subsidiary variables are involved in this model. In sequence of introduction, they are oceanic CO_2 , ocean carbonate CO_3^{2-} , bicarbonate HCO_3^- , ocean acidity via H^+ , and then oceanic calcium Ca^{2+} and calcium carbonate CaCO_3 , and finally ocean biomass and its rate limiting nutrient, taken to be phosphate. The result is a series of ordinary differential equations describing the concentrations of these substances in the world's oceans. We conclude the section with two illustrative applications, one concerning planetary cooling since the Eocene, and the other the future consequences of global warming.

3.1 The carbon cycle

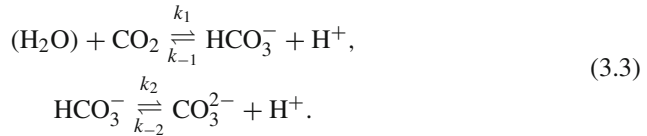
Carbon dioxide is produced from volcanoes and by weathering of organic carbon, the latter of which has in effect dramatically increased since the Industrial Revolution, by human agency. Atmospheric CO_2 is removed, largely by dissolving in the ocean, but an important amount is also lost through its dissolution in water droplets, and subsequent precipitation. Precipitation on land causes dissolution and thus weathering of rocks, from which a number of ionic species are delivered to the ocean, notably sodium, magnesium, calcium, potassium, chloride, sulphate and bicarbonate. The different ions have different residence times, and for all except bicarbonate and calcium these are very long, at 10^7 years, because they 'leak' very slowly from the ocean (for example, sodium and chloride are removed in evaporite beds). As a consequence, these 'conservative' or leakage ions provide an almost constant background (negative) charge, which is compensated by the net positive charge of the calcium and (bi-)carbonate ions, along with the acidity H^+ . The net negative charge of the conservative ions is given by

$$L_- = -[\text{Na}^+] - 2[\text{Mg}^{2+}] - [\text{K}^+] + [\text{Cl}^-] + 2[\text{SO}_4^{2-}], \quad (3.1)$$

and currently has the value (Emerson and Hedges 2008, table 2.3)

$$L_- \approx 1.74 \times 10^{-2} \text{ mol kg}^{-1}. \quad (3.2)$$

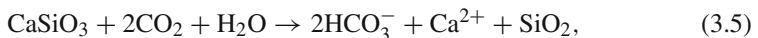
Carbon enters the ocean as dissolved CO_2 from the atmosphere, or as bicarbonate ion HCO_3^- through river flow, but in the ocean the carbon rapidly becomes partitioned to an equilibrium (buffered) between those two forms and also carbonate ion CO_3^{2-} , by means of the reactions



Water is not a limiting reactant, and so is not included in the reaction rates given below. The sum of the concentrations (denoted with square brackets) of the three species is called the dissolved inorganic carbon (DIC), and denoted C :

$$C = [\text{CO}_2] + [\text{HCO}_3^-] + [\text{CO}_3^{2-}]. \quad (3.4)$$

Carbon is added to the ocean through a river flux of bicarbonate, which is formed through the typical net reaction



the important ingredients of which for the present purpose are



that is to say one mole of atmospheric derived carbon produces one mole of bicarbonate and half a mole of calcium, which flow to the ocean. Weathering of carbonate rocks has the same effect, through the reaction



The story with calcium in the ocean is a little complicated. We need to keep track of it, because it lends a significant positive charge to the ocean, and thus dynamically affects the balance of the other ions, since the ocean as a whole is charge neutral. The calcium ions which flow into the ocean find themselves in a supersaturated (with respect to carbonate) upper layer. They thus have a proclivity to precipitate, although the supersaturation is not sufficient for them to do this via homogeneous nucleation. However, calcium also forms (organic) calcium carbonate through its uptake by coccolithophores, foraminifera and coral reefs, and we can suppose that these (particularly reefs) also act as nucleation sites for the encrusted growth of inorganic calcium carbonate.

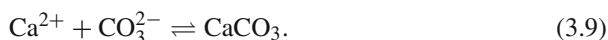
The solubility increases with pressure, and thus depth, and is such that, in the deeper parts of the ocean, redissolution of sinking dead skeletal biomass occurs, while in the shallower ocean (on the shelves, or near mid-ocean ridges) a calcite ‘snow’ rains down on the benthic sediments. Even there, some bacterial action causes further breakdown, but there is overall a net burial rate of the CaCO_3 from the ocean.

In the present day, and ever since the development of plankton with hard shells in the Triassic, much of the precipitation in the upper ocean is effected by planktonic uptake, and the sinking towards the deep ocean is caused by the deaths and settling of these organisms. The story is further complicated by the existence of continental shelves, on which dissolution cannot occur, and where an additional sink due to the growth of coral reefs occurs. As the ice sheets grow to their maximum extent, the shelves are exposed, and the resultant exposure of the carbonate rocks is liable to cause an enhancement of the weathering rate, and thus of delivery of carbon to the ocean. This enhancement is itself compensated by the reduced effectiveness of chemical weathering because of lower temperatures and CO_2 , and the two effects may roughly balance (Foster and Vance 2006), or lead to a net increase in weathering rate (Munhoven 2002).

The growth of organic calcium carbonate can be represented by the reaction



which is normally compounded with (3.3)₁. The forward reaction represents the uptake of calcium and bicarbonate by plankton, while the backward reaction represents the dissolution of calcite in the deep ocean or by respiration dissolution induced by benthic bacteria. In addition, we suppose that precipitation and dissolution of inorganic CaCO_3 will occur via the reaction

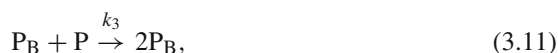


From the reactions in (3.3), we can write the net carbon buffering reaction rates as

$$\begin{aligned} R_1 &= k_1 [\text{CO}_2] - k_{-1} [\text{HCO}_3^-] [\text{H}^+], \\ R_2 &= k_2 [\text{HCO}_3^-] - k_{-2} [\text{CO}_3^{2-}] [\text{H}^+]. \end{aligned} \quad (3.10)$$

These are straightforward, but the prescription of the calcium carbonate formation rates in (3.8) and (3.9) is open to elaboration. The law of mass action is not applied to (3.8) as it stands, because neither calcium nor carbon is rate-limiting for the growth of plankton. It is most probable that it is phosphorus which is rate-limiting, and we assume this.

Uptake of phosphorus P by biomass is represented through the reaction



which represents cell growth by mitosis. P is phosphorus in solution (as phosphate ion, partitioned between PO_4^{3-} , HPO_4^{2-} , and H_2PO_4^-), while P_B is phosphorus in biomass.

When organisms die, the phosphate of the organic matter is remineralised through the back reaction



The law of mass action applied to (3.11) and (3.12) implies that rate of formation of biophosphorus is

$$r_3 = k_3[P_B][P] - k_{-3}[P_B], \tag{3.13}$$

and this is also the rate of loss of phosphate ion from sea water. To calculate the net formation rate of CaCO₃, we use the fact that biomass contains the elements carbon, phosphorus and so on in fixed proportions, called Redfield ratios. The C:P ratio in organic soft tissue is 106:1, while the C:P:Ca ratio in the total deposited organic material (including skeletal tissue) is 131:1:26 (Broecker and Peng 1982). Evidently the ratio of the skeletal CaCO₃ to soft tissue organic carbon has a ratio of about one to four, and the relevant uptake ratio of carbon/phosphorus and calcium/phosphorus into skeletal CaCO₃ is $R \approx 26$. Thus the net rate of formation of organic skeletal CaCO₃ is given by

$$R_3 = Rr_3. \tag{3.14}$$

Phosphorus is rate limiting because the flux of P to the ocean is so small. If burial of skeletal tissue were the only way of removing calcium from the ocean, calcium levels would build up because the calcium flux to the ocean is greater than 26 times the P flux. Eventually, the ocean becomes supersaturated (as it is except at great depth), and the excess is removed via precipitation through the reaction (3.9). We assume that the rate of precipitation is given by

$$R_4 = k_4 \left([Ca^{2+}] [CO_3^{2-}] - K_{cp} \right)^n \tag{3.15}$$

(Ridgwell and Zeebe 2005), where k_4 , K_{cp} and n are constants. (A similar expression applies in conditions of dissolution.)

Before writing the conservation laws for the ionic species in the ocean, we consider the balance of atmospheric CO₂. We denote the volcanic (or anthropogenic) CO₂ source to be V , with units of kgCO₂ year⁻¹, and we denote the weathering rate, measured by the removal of CO₂ in the reaction (3.5), as W , measured in units of kgCO₂ m⁻² year⁻¹. In addition, there is a flux of CO₂ to the ocean equal to $h_{CO_2}(p - p_s)$, where p is atmospheric partial pressure of CO₂, and p_s is its value at the ocean surface. The transport coefficient represents the turbulent diffusivity of the atmosphere, and has units of kgCO₂ Pa⁻¹ year⁻¹. The surface pressure p_s is related to the dissolved ocean CO₂ concentration by Henry's law:

$$p_s = \frac{[CO_2]}{K_H}. \tag{3.16}$$

The conservation law for atmospheric CO₂ mass m_{CO_2} is thus

$$\dot{m}_{\text{CO}_2} = V - A_L W - h_{\text{CO}_2}(p - p_s), \quad (3.17)$$

where A_L is total land surface area. We base our choice of weathering rate on the formula given by Walker et al. (1981):

$$W = W_0 \left(\frac{p}{p_0} \right)^\mu \exp \left[\frac{T - T_0}{\Delta T_c} \right]. \quad (3.18)$$

The choice of parameters corresponds to present day weathering rates, and increases with T and p , as is realistic.

To relate m_{CO_2} to the CO₂ partial pressure p , we use Dalton's law, which states that

$$\frac{p}{p_a} = \frac{m_{\text{CO}_2} M_a}{M_{\text{CO}_2} m_a}, \quad (3.19)$$

where M_a is the molecular weight of air, M_{CO_2} is the molecular weight of CO₂, and m_a is the mass of the atmosphere, related to the atmospheric pressure p_a by

$$p_a = \frac{m_a g}{A_E}, \quad (3.20)$$

where A_E is Earth's surface area. From these it follows that (3.17) takes the form

$$\frac{A_E}{M_a g} \dot{p} = \frac{V - A_L W - h_{\text{CO}_2}(p - p_s)}{M_{\text{CO}_2}}, \quad (3.21)$$

with the units of each side now being moles per year. Finally, if $m_{oc} = \rho_{\text{H}_2\text{O}} V_{oc}$ is the mass of the ocean, then (3.21) can be written in the form

$$\frac{A_E}{M_a g m_{oc}} \dot{p} = v - A^* W - h(p - p_s), \quad (3.22)$$

where we define

$$A^* = \frac{A_L}{m_{oc} M_{\text{CO}_2}}, \quad h = \frac{h_{\text{CO}_2}}{m_{oc} M_{\text{CO}_2}}, \quad v = \frac{V}{m_{oc} M_{\text{CO}_2}}. \quad (3.23)$$

The units of (3.22) are now M year⁻¹, where 1 M = 1 mole kg⁻¹ is the standard concentration unit for oceanic ionic species.

In terms of the reactions defined in (3.10), we can now write down the equations for the concentrations of the chemical species. The units of concentration are M, and

reaction-conservation laws for the reactants are

$$\begin{aligned}
 [\dot{\text{CO}}_2] &= -R_1 + h(p - p_s), \\
 [\dot{\text{CO}}_3^{2-}] &= R_2 - R_4, \\
 [\dot{\text{HCO}}_3^-] &= R_1 - R_2 - R_3 + A^*W, \\
 [\dot{\text{H}}^+] &= R_1 + R_2 + R_3, \\
 [\dot{\text{Ca}}^{2+}] &= -R_3 - R_4 + \frac{1}{2}A^*W, \\
 [\dot{\text{CaCO}}_3] &= R_3 + R_4 - B[\text{CaCO}_3], \\
 [\dot{\text{P}}] &= -r_3 + \rho A^*W, \\
 [\dot{\text{P}}_B] &= r_3 - B[\text{P}_B],
 \end{aligned}
 \tag{3.24}$$

where we take account of the fact that the weathering reaction loses A^*W moles per year of atmospheric carbon, and each such mole produces an oceanic influx of one mole of bicarbonate and half a mole of calcium. The burial coefficient B is taken to be the inverse of the residence time t_C of carbon in the ocean,

$$B = \frac{1}{t_C},
 \tag{3.25}$$

and ρ is the molar ratio of P to C weathering rates.

In writing (3.24), we have tacitly assumed that the ocean volume is constant. At the last glacial maximum, sea level was lower than today's by about 120 m; since the mean ocean depth is about 3,700 m, this represents a change of about 3 %, and it seems that the volume change can be neglected at leading order. We assume this for the moment, but will return to the issue later.

Simplification

The reactions of the bicarbonate buffering system are fast, occurring in minutes. More specifically, the time scale for CO_2 adjustment is $k_1^{-1} \sim 30$ s, and that for HCO_3^- is $k_2^{-1} \sim 0.017$ s, where these values are given by Zeebe and Wolf-Gladrow (2001, p. 110: note that $k_2 = k_{-5}^{\text{H}^+}$ in their table). This implies that the coefficients in the terms R_1 and R_2 are large, and consequently the equations in which those terms appear rapidly approach a quasi-equilibrium in which, approximately, $R_1 = R_2 = 0$, whence

$$[\text{HCO}_3^-] = \frac{K_1 Y}{X}, \quad [\text{CO}_3^{2-}] = \frac{K_2 [\text{HCO}_3^-]}{X} = \frac{K_1 K_2 Y}{X^2},
 \tag{3.26}$$

where we write

$$X = [\text{H}^+], \quad Y = [\text{CO}_2],
 \tag{3.27}$$

and the equilibrium constants K_i are defined by

$$K_1 = \frac{k_1}{k_{-1}}, \quad K_2 = \frac{k_2}{k_{-2}}. \quad (3.28)$$

Now, the first four equations in (3.24) are all approximated by the two equilibria in (3.26). The missing two equations are found by taking suitable linear combinations of the equations to eliminate R_1 and R_2 . In particular, defining the dissolved inorganic carbon C via (3.4), and the net positive charge L_+ of the active ions (calcium and carbon species) as

$$L_+ = [\text{H}^+] + 2[\text{Ca}^{2+}] - [\text{HCO}_3^-] - 2[\text{CO}_3^{2-}], \quad (3.29)$$

then from (3.24) we have the exact equations

$$\begin{aligned} \dot{C} &= h(p - p_s) + A^*W - R_3 - R_4, \\ \dot{L}_+ &= 0, \end{aligned} \quad (3.30)$$

whence we may take

$$L_+ = L_-, \quad (3.31)$$

corresponding to charge neutrality.¹

In terms of C , (3.26) implies

$$Y \left[1 + \frac{K_1}{X} + \frac{K_1 K_2}{X^2} \right] = C, \quad (3.32)$$

and then from (3.31), after a little algebra, we obtain the equation for $X = [\text{H}^+]$ in the form

$$X - \frac{K_1(X + 2K_2)C}{X^2 + K_1X + K_1K_2} = L_- - 2Z, \quad (3.33)$$

where we define

$$Z = [\text{Ca}^{2+}]. \quad (3.34)$$

It is useful to take advantage of the observed values of the variables in Table 1 to simplify this expression. We see that $X \ll K_1$, and equality only occurs for $\text{pH} = 5.9$,

¹ In a more complete discussion, we might also consider the charge of the various phosphate ions, but the concentrations are so small that this makes no effective difference.

Table 1 Present estimates of the equilibrium constants K_i and the ionic species concentrations in units of M (1 M = 1 mole kg^{-1}) (Emerson and Hedges 2008)

Species/constant	Typical value (M)
$[\text{Ca}^{2+}] = Z$	1.03×10^{-2}
$[\text{CO}_2] = Y$	0.8×10^{-5}
$[\text{CO}_3^{2-}] \approx S$	0.24×10^{-3}
$[\text{H}^+] = X$	0.63×10^{-8}
$[\text{HCO}_3^-] \approx Q$	1.7×10^{-3}
[P]	3×10^{-6}
K_1	1.4×10^{-6}
K_2	1.1×10^{-9}
C	2.0×10^{-3}
L_-	1.74×10^{-2}

C is dissolved inorganic carbon, and L_- is net negative charge equivalent of the conservative ions (see (3.1))

a strongly acid ocean. Assuming $\text{pH} \gtrsim 7$ (present day ocean values are ≈ 8.2), then $X \ll K_1$, and the solution of (3.33) is approximately

$$[\text{H}^+] = X \approx \frac{K_2 Q}{S}, \tag{3.35}$$

where we define

$$S = 2Z - L_- - C, \quad Q = L_- + 2C - 2Z. \tag{3.36}$$

Both quantities are necessarily positive; present estimates are that both are of order 10^{-3} M. With the same approximation, we have

$$[\text{CO}_2] = Y = \frac{K_2 Q^2}{K_1 S}, \tag{3.37}$$

and also, noting that $X \ll Y \ll Z$,

$$[\text{CO}_3^{2-}] \approx S, \quad [\text{HCO}_3^-] \approx Q, \tag{3.38}$$

which give more precise estimates for S and Q .

3.2 The ocean-atmosphere model

Combining the equations (3.13), (3.14), (3.15), (3.16), (3.22), (3.24)_{5,6}, (3.30)₁, (3.37) and (3.38), and defining also

$$N = [\text{CaCO}_3], \quad P = [\text{P}], \tag{3.39}$$

we obtain the equations

$$\begin{aligned}
 \frac{A_E}{M_{agm_{oc}}} \dot{p} &= -A^*W + v - h(p - p_s), \\
 \dot{C} &= h(p - p_s) + A^*W - R_3 - R_4, \\
 \dot{Z} &= \frac{1}{2}A^*W - R_3 - R_4, \\
 \dot{N} &= R_3 + R_4 - BN, \\
 R\dot{P} &= -R_3 + \rho RA^*W, \\
 R\dot{P}_B &= R_3 - BRP_B,
 \end{aligned}
 \tag{3.40}$$

where also

$$p_s \approx \frac{K_2 Q^2}{K_1 K_H S}, \quad R_3 = (k_3 P - k_{-3})RP_B, \quad R_4 \approx k_4 (ZS - K_{cp})^n,$$

$$Q = L_- + 2C - 2Z, \quad S = 2Z - L_- - C.
 \tag{3.41}$$

It is easy to show from these equations that if $S, Q > 0$, as they must be, then they remain so, whatever the size (or sign) of L_- .

In addition, we suppose that the solubility K_H and bioreaction rate k_3 will depend on temperature, and this suggests that we define a dimensionless solubility κ_H and dimensionless bioreaction rate κ_3 by writing

$$\begin{aligned}
 K_H &= K_H^0 \kappa_H, & \kappa_H &= \exp[-b_H(T - T_0)], \\
 k_3 &= k_3^0 \kappa_3, & \kappa_3 &= \exp[b_3(T - T_0)],
 \end{aligned}
 \tag{3.42}$$

where K_H^0 is a scale for the CO₂ solubility coefficient, and k_3^0 is a scale for the bioreaction rate. This allows us to study the effect of the solubility pump, in which κ_H is a decreasing function of temperature, and also, in due course, the effect of thermally enhanced bioproductivity, in which κ_3 is an increasing function of T . The dependence of biomass on temperature via the coefficient b_3 will turn out to be crucial in producing the CO₂ record, but our initial discussion will ignore it (reflecting the historical evolution of our study).

The values of the constants in the model are give in Table 2. The choice of some of these values is explained below. The carbon buffering rates k_{-1} and k_{-2} are given in terms of k_1^{-1}, k_2^{-1} , and the ratios K_i . The estimate of b_3 is based on a doubling of bioactivity every ten degrees. The value of h is computed by assuming that the present interfacial flux, around 2 GtC year⁻¹, corresponding to a volumetric rate of increase in the ocean of 1.2×10^{-7} M year⁻¹, arises from a difference Δp between present day (2000) $p \approx 37$ Pa (Emerson and Hedges 2008, table 11.1), and pre-industrial (<1800) $p \approx 28$ Pa; thus $h\Delta p = 1.2 \times 10^{-7}$ M year⁻¹, whence the value in Table 2.

Table 2 Values of the constants in the model

Symbol	Meaning	Typical value
A^*	Weathering scale coefficient	$0.25 \times 10^{-5} \text{ M m}^2 \text{ kg}^{-1}$
A_E	Planetary surface area	$5.1 \times 10^{14} \text{ m}^2$
A_L	Land surface area	$1.5 \times 10^{14} \text{ m}^2$
B	Carbon burial rate	$10^{-5} \text{ year}^{-1}$
b_H	Carbon solubility exponent	0.029 K^{-1}
b_3	Bioactivity exponent	0.069 K^{-1}
g	Acceleration due to gravity	9.81 m s^{-2}
h	Interfacial transport coefficient	$1.3 \times 10^{-8} \text{ M Pa}^{-1} \text{ year}^{-1}$
k_1^{-1}	CO_2 reaction time	30 s
k_2^{-1}	HCO_3^- reaction time	0.017 s
k_3^0	Biomass calcium uptake rate	$51 \text{ M}^{-1} \text{ year}^{-1}$
k_4	CaCO_3 precipitation coefficient	$2.1 \times 10^{-3} \text{ M}^{-(2n-1)} \text{ year}^{-1}$
k_{-3}	CaCO_3 dissolution rate	$1.4 \times 10^{-4} \text{ year}^{-1}$
K_H^0	Henry's law coefficient	$4.5 \times 10^{-7} \text{ M Pa}^{-1}$
K_{cp}	CaCO_3 solubility coefficient	$0.5 \times 10^{-6} \text{ M}^2$
m_{oc}	Ocean mass	$1.38 \times 10^{21} \text{ kg}$
M_a	Molecular weight of air	$2.88 \times 10^{-2} \text{ kg mole}^{-1}$
M_{CO_2}	Molecular weight of CO_2	$4.4 \times 10^{-2} \text{ kg mole}^{-1}$
n	CaCO_3 solubility exponent	1
p_0	Atmosphere CO_2 scale	28 Pa
R	Redfield calcium ratio	26
t_C	Oceanic carbon residence time	10^5 year
T_0	Reference temperature	288 K
v	Scaled CO_2 production rate	$0.5 \times 10^{-8} \text{ M year}^{-1}$
V	CO_2 production rate	$3 \times 10^{11} \text{ kg year}^{-1}$
V_{oc}	Ocean volume	$1.35 \times 10^{18} \text{ m}^3$
W_0	Weathering scale	$4 \times 10^{-3} \text{ kg CO}_2 \text{ m}^{-2} \text{ year}^{-1}$
ΔT_c	Weathering temperature scale	13 K
μ	Weathering exponent	0.3
ρ	P:C weathering ratio	0.4×10^{-2}
$\rho_{\text{H}_2\text{O}}$	Density of sea water	$1.025 \times 10^3 \text{ kg m}^{-3}$

We define a molar concentration as $1 \text{ M} = 1 \text{ mole kg}^{-1}$

To progress further, we non-dimensionalise the equations. Over time scales less than 10 My, we may take L_- to be constant. The non-dimensionalisation is a little subtle, because we note from Table 1 that Q and S are a good deal smaller than L_- and Z . Therefore we consider first the steady state of the system, in order to find the best choice of scales.

We anticipate that the time derivative term for p is small, and the interfacial transfer term is large. Then generally, $p \approx p_s$ while also $h(p - p_s) + A^*W \approx v$, so that

$$\dot{C} \approx v - R_3 - R_4. \tag{3.43}$$

In the steady state, we thus have

$$R_3 + R_4 = v = \frac{1}{2}A^*W = BN, \quad R_3 = \rho RA^*W = BRP_B, \tag{3.44}$$

and thus

$$R_3 = 2\rho Rv, \quad P_B = \frac{2\rho v}{B}. \tag{3.45}$$

Net calcite precipitation occurs ($R_4 > 0$) if $\rho R < \frac{1}{2}$, consistent with the values in Table 2. The weathering term is discussed further below, but it depends on p as well as temperature, and we may suppose that we can choose the value of $p = p_0$ to ensure that $v = \frac{1}{2}A^*W$. A value of $p_0 = 28$ Pa is implied by the assumption that pre-industrial weathering was approximately in balance with volcanic output. (Later we shall find that a larger value seems more appropriate.) Since also $p \approx p_s$, this implies that

$$\frac{Q^2}{S} \approx \frac{K_1 K_H p_0}{K_2} \approx 1.2 \times 10^{-2} \text{ M} \tag{3.46}$$

(which it is). In addition, we have

$$N = \frac{v}{B} \tag{3.47}$$

in a steady state.

Equilibrium of the C equation requires

$$R_3 + R_4 = (k_3 P - k_{-3})RP_B + k_4(ZS - K_{cp})^n = v, \tag{3.48}$$

while that of the P equation requires

$$R_4 = k_4(ZS - K_{cp})^n = v - R_3 = (1 - 2\rho R)v. \tag{3.49}$$

The terms $k_3 P RP_B + k_4(ZS - K_{cp})^n$, $k_{-3} RP_B$, v represent, respectively, biomass uptake of calcium, dissolution of organic calcium carbonate, and burial, and are thought presently to have ratios of 4:3:1 (Zeebe and Westbroek 2003). This suggests $k_{-3} \approx \frac{3B}{2\rho R} = 1.4 \times 10^{-4} \text{ year}^{-1}$, and using present day values of $[P] \sim 3 \times 10^{-6} \text{ M}$, we find $k_3 \approx 51 \text{ M}^{-1} \text{ year}^{-1}$.

In the upper ocean, the supersaturation is approximately $\frac{ZS}{K_{cp}} \approx 4.8$, from which it follows that we can estimate $K_{cp} \approx 0.5 \times 10^{-6} \text{ M}^2$. Present day P input to the oceans

is estimated as $1.7 \times 10^9 \text{ kg year}^{-1}$, corresponding to $0.4 \times 10^{-10} \text{ M year}^{-1}$, and since $v \approx 0.5 \times 10^{-8} \text{ M year}^{-1}$, this suggests $\rho = 0.4 \times 10^{-2}$. Finally, equality in (3.49) implies (taking $n = 1$) that $k_4 \approx 2.1 \times 10^{-3} \text{ M}^{-1} \text{ year}^{-1}$.

The discussion above suggests that we write the model equations (3.40) in terms of $Q \approx [\text{HCO}_3^-]$ and $S \approx [\text{CO}_3^{2-}]$; from (3.41) and (3.40), we then have

$$\begin{aligned} \frac{A_E}{M_a g m_{oc}} \dot{p} &= -A^*W + v - h(p - p_s), \\ \dot{Q} &= 2h(p - p_s) + A^*W, \\ \dot{S} &= -h(p - p_s) - R_3 - R_4, \\ \dot{N} &= R_3 + R_4 - BN, \\ R\dot{P} &= -R_3 + \rho RA^*W, \\ R\dot{P}_B &= R_3 - BRP_B. \end{aligned} \tag{3.50}$$

Now we scale the variables by writing

$$\begin{aligned} N &\sim \frac{v}{B}, \quad Q \sim Q_0, \quad S \sim S_0, \quad R_3 = \frac{2k_{-3}\rho Rv}{B} u_b, \quad R_4 = vu_p, \\ P &\sim \frac{k_{-3}}{k_3^0}, \quad P_B \sim \frac{2\rho v}{B}, \quad t \sim \frac{1}{B}, \quad p \sim p_s \sim p_0, \quad W = W_0w, \quad T = T_0 + \Delta T_c\theta, \end{aligned} \tag{3.51}$$

where

$$S_0 = \frac{2v}{k_4L_-}, \quad Q_0 = \left(\frac{2K_1K_H^0p_0v}{k_4L_-K_2} \right)^{1/2}. \tag{3.52}$$

The non-dimensional forms of the equations are (we retain the same symbols for the dimensionless variables)

$$\begin{aligned} \varepsilon \dot{p} &= 1 - \Omega w - \Lambda(p - p_s), \\ \eta \dot{Q} &= 2\Lambda(p - p_s) + \Omega w, \\ v \dot{S} &= -\beta u_b - u_p - \Lambda(p - p_s), \\ \dot{N} &= \beta u_b + u_p - N, \\ \zeta \dot{P} &= -u_b + \frac{\gamma \Omega w}{\beta}, \\ 2\gamma \dot{P}_B &= \beta u_b - 2\gamma P_B, \end{aligned} \tag{3.53}$$

where

$$\begin{aligned}
 p_s &= \frac{Q^2}{\kappa_H S}, \quad \kappa_H = \exp(-b\theta), \\
 u_b &= (\kappa_3 P - 1) P_B, \quad \kappa_3 = \exp(b'\theta), \\
 u_p &= S(1 + \delta_1 Q + \delta_2 S) - \Sigma, \\
 w &= p^\mu e^\theta,
 \end{aligned}
 \tag{3.54}$$

and the dimensionless parameters are defined by

$$\begin{aligned}
 \Omega &= \frac{A^* W_0}{v}, \quad \eta = \frac{B Q_0}{v}, \quad \nu = \frac{B S_0}{v}, \quad \Lambda = \frac{h p_0}{v}, \\
 \beta &= \frac{2\rho R k_{-3}}{B}, \quad \delta_1 = \frac{Q_0}{L_-}, \quad \delta_2 = \frac{2S_0}{L_-}, \quad \varepsilon = \frac{A_E p_0 B}{M_a g m_{oc} v}, \\
 b &= b_H \Delta T_c, \quad b' = b_3 \Delta T, \quad \zeta = \frac{B^2}{2\rho k_3 v}, \quad \gamma = \rho R, \quad \Sigma = \frac{k_4 K_{cp}}{v}.
 \end{aligned}
 \tag{3.55}$$

Using these estimates, we calculate values of Q_0 and S_0 as defined in (3.52) to be

$$Q_0 = 1.8 \times 10^{-3} \text{ M}, \quad S_0 = 0.27 \times 10^{-3} \text{ M}.
 \tag{3.56}$$

The residence time scale for carbon (thus C) is taken as 10^5 year (Emerson and Hedges 2008). From (3.40)₃, this suggests a residence time for calcium of $\sim \frac{1}{k_4 S_0} = \frac{L_-}{2v}$, which with these estimates is 1.7 My, comparable to Emerson and Hedges' estimate of 1.2 My.

Now we use these values to estimate the size of the dimensionless parameters. They are

$$\begin{aligned}
 \Omega &\sim 2, \quad \eta \sim 3.6, \quad \nu \sim 0.54, \quad \Lambda \sim 70.2, \\
 \varepsilon &\sim 0.07, \quad \delta_1 \sim 0.1, \quad \delta_2 \sim 0.03, \quad \beta \sim 3, \\
 b &\sim 0.38, \quad b' \sim 0.9, \quad \zeta \sim 0.05, \quad \gamma \sim 0.1, \quad \Sigma \sim 0.21.
 \end{aligned}
 \tag{3.57}$$

The fact that $\Lambda \gg 1$ tells us that as far as atmospheric CO_2 is concerned, it adjusts rapidly, on a dimensionless time scale $t \sim \frac{\varepsilon}{\Lambda}$, to a quasi-steady state in which $p \approx p_s$, and more precisely

$$\Lambda(p - p_s) \approx 1 - \Omega w;
 \tag{3.58}$$

the dimensional time scale over which this relaxation occurs is

$$t_{\text{CO}_2} = \frac{A_E}{M_a g m_{oc} h} \approx 100 \text{ year}.
 \tag{3.59}$$

Next, P reaches quasi-equilibrium rapidly on a time scale of $O(\zeta)$. In this equilibrium,

$$\beta u_b \approx \gamma \Omega w, \quad P \approx \frac{1}{\kappa_3} \left(1 + \frac{\gamma \Omega w}{\beta P_B} \right); \tag{3.60}$$

the dimensional time scale over which P relaxes is

$$t_P = \frac{B}{2\rho k_3 v} \approx 5,000 \text{ year}. \tag{3.61}$$

We note from (3.54) that

$$u_p \approx S - \Sigma. \tag{3.62}$$

On time scales longer than t_P we can use (3.58) and (3.60), and write (3.53) in the approximate form

$$\begin{aligned} \eta \dot{Q} &= 2 - \Omega w, \\ v \dot{S} &= \Omega(1 - \gamma)w - (1 - \Sigma) - S, \\ \dot{N} &= \gamma \Omega w + S - \Sigma - N, \\ \dot{P}_B &= \frac{1}{2} \Omega w - P_B. \end{aligned} \tag{3.63}$$

In our estimates, $\gamma < 1$, and this is necessary since $\gamma = \rho R$; if $\gamma > 1$, it implies that P is not rate limiting, and the reaction rates would be necessarily different.

Solutions of (3.63) tend to a steady state, which can be described as follows. We will take the CO_2 solubility to be constant, i.e., $\kappa_H = 1$ (the effect of its variation with temperature will be studied later). Also for the moment we take $\kappa_3 = 1$. On a time scale $t \sim v$, corresponding to 50,000 years, S (carbonate ion) relaxes to a quasi-equilibrium in which, since $w \sim p^\mu \sim \left(\frac{Q^2}{S}\right)^\mu$,

$$\Omega(1 - \gamma) \left(\frac{Q^2}{S}\right)^\mu - S = 1 - \Sigma. \tag{3.64}$$

The left-hand side is a monotonically decreasing function of S , and it follows that S tends to a unique positive value which depends on Q such that $S(Q)$ is monotonically increasing. For small Q ,

$$S \approx \left\{ \frac{\Omega(1 - \gamma)}{1 - \Sigma} \right\}^{1/\mu} Q^2, \quad w \approx \left\{ \frac{1 - \Sigma}{\Omega(1 - \gamma)} \right\}, \tag{3.65}$$

while for large Q

$$S \approx \{\Omega(1 - \gamma)\}^{\frac{1}{\mu+1}} Q^{\frac{2\mu}{\mu+1}}, \quad w \approx S. \tag{3.66}$$

The weathering rate w is thus an increasing function of Q , so that on the longer time scale $t = O(\eta)$, Q relaxes to equilibrium, and the whole system is at steady state, in which

$$\Omega w = 2, \quad N = 1, \quad S = 1 + \Sigma - 2\gamma. \tag{3.67}$$

In the absence of any ice-related feedback, this simple model suggests that the carbon/calcium buffering system responds stably to alterations in weathering rate. Figure 3 shows these successive relaxations of the model using the parameters given in Tables 1 and 2.

3.3 An application to post-Eocene cooling

We can explain the cooling of the planet since the Eocene by supposing that the uplift of the Himalayas has caused an amplification of the specific weathering rate (the parameter W_0), and thus Ω . Alternatively, the closure of the Tethys Ocean and the

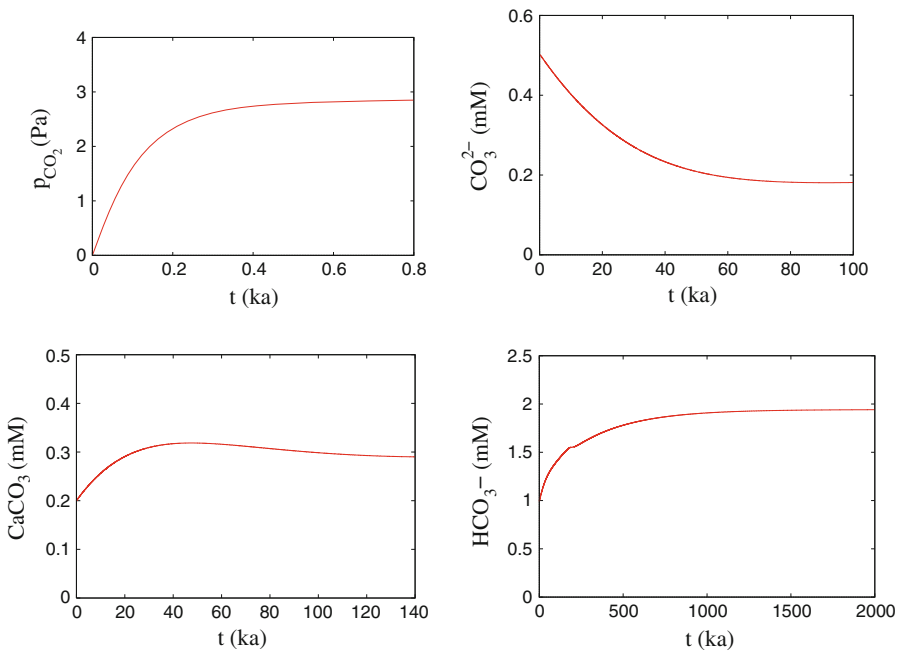


Fig. 3 Relaxation of atmospheric $p = p_{\text{CO}_2}$, $S \approx [\text{CO}_3^{2-}]$, $N = [\text{CaCO}_3]$ and $Q \approx [\text{HCO}_3^-]$ over a range of different time scales. Concentration units are mM, while those for atmospheric CO_2 are Pa. Time is measured in ka (10^3 year). Note the different time scales for the four variables. The initial values chosen were $p = 0$ Pa, $S = 0.5$ mM, $N = 0.2$ mM, $Q = 1$ mM, $P = 1$ μM and $P_B = 0.1$ μM . Note that the apparent equilibria for p , S and N are only interim values; the final steady states at 2 Ma are $p \approx 28$ Pa, $S \approx 0.24$ mM, $Q \approx 1.94$ mM and $N \approx 0.5$ mM. P (not shown) grows for 170 ka, during which time biomass is absent, then P_B grows on a time scale of 30 ka and P declines, with their final equilibria being $P \approx 2.94$ μM , $P_B \approx 4$ μM

consequent decreasing subduction and then arc volcanism of the carbonate-rich continental shelves has led to a decline in volcanic carbon production v , which also (see (3.55)) causes an increase in Ω . In fact these two processes are related consequences of the same tectonic collision. If Ω has increased since the Eocene, then in order to retain the balance in (3.67), CO_2 pressure must be reduced, and this causes cooling. In turn, (3.37) implies that Q^2/S has decreased.

It may also be reasonable to suppose that increased weathering has caused increased production of positive conservative ions, and in this case L_- has decreased since the Eocene. Consequently, (3.52) implies that the carbonate ion S has increased. It then follows from (3.35) that $[\text{H}^+]$ has decreased, i.e., ocean acidity has decreased. It is less obvious in what way bicarbonate Q has changed, since in (3.52) both p_0 and L_- have decreased.

3.4 An application to global warming

As a parenthetical remark, note that the current anthropogenic release of CO_2 has the effect of increasing the value of v in the model. This has the confusing effect of changing all the scales, so it is easier to see what happens by consulting the dimensional equations (3.50). If we take the anthropogenic value to be v_A (and currently $v_A \approx 70v$), then on a time scale of $t_{\text{CO}_2} = 100$ year, p relaxes to the approximate dimensional value

$$p \approx p_s + \frac{v_A}{h} = p_0 \left(1 + \frac{v_A}{\Lambda v} \right), \tag{3.68}$$

if $p_s = p_0$ pre-industrially. Taking $v_A = 70v$ gives an equilibrated atmospheric p of 56 Pa, or about 560 ppmv. This is (apparently: wait) the good news. The bad news is that this may be comparable to the level at which the continent wide Antarctic Ice Sheet became established 34 My ago (Pagani et al. 2011) suggest a threshold for onset around 800 ppm). If that is the case, and bearing in mind the hysteretic response to climate, then we may already be in a situation where the major ice sheets are beginning to change dramatically. The recent observations of Pine Island Glacier retreat and the speed-up of Jakobshavn Isbrae are noteworthy in this context. If these observations represent the signature of an initial collapse of the ice sheets, then, given that the last ice age raised sea level by 120 m in 10 ky, we might expect the present approximate equivalent of 66 m of sea level held in Greenland and Antarctica to last about 5 ky, leading to sea level rising at a metre per century.

Consulting (3.50), the ocean carbonate ion starts to drop rapidly; approximately,

$$\dot{S} = -v_A. \tag{3.69}$$

In a time of order

$$t_A = \frac{S}{v_A} \approx 700 \text{ year}, \tag{3.70}$$

the carbonate ion approaches zero, by which time the ocean has become undersaturated with carbonate. Simultaneously, bicarbonate increases rapidly:

$$\dot{Q} \approx 2v_A. \tag{3.71}$$

The carbon buffering system causes drastic increase in ocean acidity (see (3.35)), and dissolved CO₂ (see (3.37)), which leaks into the atmosphere, causing massive further rise in temperature. To see what happens after this we return to (3.33). Defining

$$A = 2Z - L_-, \tag{3.72}$$

we see from (3.33) and (3.26) that for $X \sim K_1$, when $C > A$, we have

$$\begin{aligned} [\text{H}^+] &\sim \frac{K_1(C - A)}{A}, & [\text{CO}_2] &\sim C - A, \\ [\text{CO}_3^{2-}] &\sim \frac{K_2 A^2}{K_1(C - A)}, & [\text{HCO}_3^-] &\approx A; \end{aligned} \tag{3.73}$$

thus in fact carbonate continues to decrease while total DIC increases, but the carbon fills up the dissolved CO₂ reservoir, with the bicarbonate being unaffected, due to the increasing acidity of the oceans.

There appears to be nothing to stop this process so long as there is no sink in the ocean. Biomass burial will finish as extinction proceeds, and because the carbonate remains undersaturated, no removal can occur in the ocean. The atmospheric CO₂ would rise inexorably, perhaps until the oceans boil, and the planet begins its long transformation into a Venusian world. This slightly gloomy prognosis must of course be qualified: it is only a consequence of this particular model. One may suppose that total carbon stocks are finite, and the carbonate run down is not maintained; the model assumes a well-mixed ocean, but in fact the mixing itself takes thousands of years, which will alleviate the process. A worse prospect is that increased storminess leads to massive increase of water vapour in the atmosphere, and this can lead to a runaway greenhouse effect.

The elephant in the room is the carbon in the ocean, which will cause unprecedented rise in atmospheric CO₂ levels on time scales of centuries. But once the carbonate alkalinity changes in this way, it will take much longer for recovery to occur should production cease; this idea is not new, and has been proposed by Archer et al. (1997).

4 Climate and ice sheet models

Preamble

In the previous section, we constructed a simple box model of the carbon cycle. In this section, we first use a simple energy balance model to relate the planetary temperature to the atmospheric CO₂ partial pressure and the ice albedo (reflectivity) of the (northern hemisphere) ice sheets. The time scale is so short that temperature is then related

algebraically to CO₂ and ice volume. Secondly, we devise a simple model of plastic ice sheet flow which allows a model for ice sheet extent to be written as an ordinary (though complicated) differential equation, which exhibits a hysteretic response to changing temperatures.

4.1 A simple climate model

The simple ocean model is now augmented by an energy balance model for the Earth surface temperature T , together with a prognostic equation for ice sheet extent l . We begin with the energy balance equation. Figure 4 shows a typical breakdown of the radiative balance in the Earth's atmosphere, see for example Fowler (2011, p. 70). The numbers indicate the fraction of the incoming short wave radiation which is reflected, absorbed or transmitted in the atmosphere. If Q_s denotes the short wave radiation from the sun, then $\frac{1}{4}Q_s$ is the average value received at the surface. A fraction f of this is absorbed by the atmosphere, and a fraction a (the albedo) is reflected back into space; the remaining $1 - a - f$ reaches the Earth's surface.

The long wave radiation budget is parcelled up as follows. An amount q_s^+ is radiated upwards from the surface and is absorbed by the atmosphere, while an amount q_d^+ from the surface is radiated to space. The atmosphere absorbs the fraction f from incoming short wave radiation as well as q_s^+ from the surface, a fraction 0.3 from latent and sensible heat, and emits q_a^+ upwards to space, and q_a^- downwards to the surface. Sensible and latent heat fluxes may be described by effective heat transport coefficients at the surface. If T_L is the mean land surface temperature and T_S the mean sea surface temperature, then we suppose the mean (mostly sensible) heat flux from the land is $h_L(T_L - T)$, while that (mostly latent) from the sea is $h_{oc}(T_S - T)$. We can then write an energy balance model for the Earth's atmosphere as

$$m_a c_a \dot{T} = A_E [\frac{1}{4} f Q_s - q_a] + \{h_{oc} A_{oc} (T_S - T) + h_L A_L (T_L - T)\}, \quad (4.1)$$

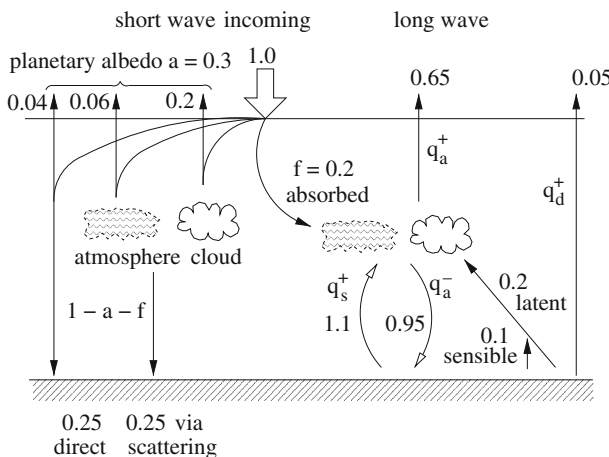


Fig. 4 Radiative energy balance for the Earth's atmosphere

where m_a is the mass of the atmosphere, c_a is the specific heat of air, A_E , A_{oc} and A_L represent Earth, ocean and land surface areas, and

$$q_a = q_a^- + q_a^+ - q_s^+ \tag{4.2}$$

is the net radiative loss from the atmosphere. Note that q_a corresponds to a fraction 0.5 of the total incoming short wave radiation.

The mean land and sea temperatures are determined by energy balances at the surface, which take the respective forms

$$\begin{aligned} \frac{1}{4}(1 - a - f)Q_s - h_L(T_L - T) - q_s &= G, \\ \frac{1}{4}(1 - a - f)Q_s - h_{oc}(T_S - T) - q_s &= G, \end{aligned} \tag{4.3}$$

where G is the mean geothermal heat flux, and

$$q_s = q_s^+ - q_a^- + q_d^+ \tag{4.4}$$

is the net radiative flux from the surface, corresponding to 0.2 of the short wave input. The equations in (4.3) act as boundary conditions for the Earth internal temperature and the ocean internal temperature. In particular, we can also write an energy balance equation similar to (4.1) for the mean ocean temperature, but do not do so here.

The geothermal heat flux is small and can be neglected. Substituting (4.3) into (4.1) then leads to the energy balance equation in the form

$$\frac{m_a c_a \dot{T}}{A_E} = \frac{1}{4}(1 - a)Q_s - q, \tag{4.5}$$

where

$$q = q_a + q_s. \tag{4.6}$$

The radiative fluxes q_a and q_s are determined by a radiative heat transfer calculation in the atmosphere, which gives them, in principle, in terms of the surface temperature. In the absence of an atmosphere, we would have black body radiation $q_s = \sigma T^4$, $q_a = 0$, thus $q = \sigma T^4$, where σ is the Stefan-Boltzmann constant, and we assume that the effect of the atmosphere is to alter this by introduction of a greenhouse coefficient $\Gamma > 0$, such that

$$q = \sigma e^{-\Gamma} T^4, \tag{4.7}$$

so that

$$c\dot{T} = \frac{1}{4}Q_s(1 - a) - \sigma e^{-\Gamma} T^4, \tag{4.8}$$

where

$$c = \frac{m_a c_a}{A_E} \tag{4.9}$$

is a measure of atmospheric thermal capacity. Values of the parameters are given in Table 3, and it is easy to show that the response time of T is very fast: around nine days for (4.8). Therefore we can suppose that this equation is in equilibrium, and for relatively small temperature perturbations ΔT corresponding to perturbations Δp in atmospheric CO₂ and ΔI in ice extent, we have

$$\Delta T \approx \frac{\frac{T}{4} \left[\Gamma_p \Delta p - \frac{a_I}{1-a} \Delta I \right]}{1 + \frac{T}{4} \left\{ \frac{a_T}{1-a} - \Gamma_T \right\}}. \tag{4.10}$$

In this equation we assume that planetary albedo a is a function of I (via the ice-albedo effect) and T (through the cloud albedo effect, the magnitude of which depends on water vapour and thus temperature), and we assume that the greenhouse coefficient Γ is a function of p (via the greenhouse effect of CO₂) and T (via the greenhouse effect of clouds and water vapour, again due to T).

All of the partial derivatives Γ_p , Γ_T , a_T and a_I should be positive. The terms in the denominator reflect the conflicting and uncertain feedback effects of clouds on the temperature. Present estimates (based on a doubling of CO₂) suggest that

$$\frac{1}{4} T \Gamma_p p_0 \sim 1.2 \text{ K}, \quad 1 + \frac{1}{4} T \left\{ \frac{a_T}{1-a} - \Gamma_T \right\} \sim 0.44 \tag{4.11}$$

(Houghton 2009, p. 30), although the dependence on p is more nearly logarithmic (Houghton 2009, p. 46), so that the CO₂ part of (4.10) may be better represented as

Table 3 Values of additional constants in the climate model

Symbol	Meaning	Typical assumed value
a	Planetary albedo	0.3
c	Thermal capacity	$10^7 \text{ J m}^{-2} \text{ K}^{-1}$
c_a	Specific heat of air	$10^3 \text{ J kg}^{-1} \text{ K}^{-1}$
m_a	Mass of atmosphere	$0.52 \times 10^{19} \text{ kg}$
Q_s	(total) Solar insolation	1370 W m^{-2}
γ_0	CO ₂ coefficient	4.65×10^{-4}
Γ	Greenhouse coefficient	see (4.8)
θ_I	Ice albedo temperature rise scale	5 K
θ_p	CO ₂ temperature rise scale	4.3 K
σ	Stefan–Boltzmann constant	$5.67 \times 10^{-8} \text{ W m}^{-2} \text{ K}^{-4}$

$$\Delta T_p = \theta_p \ln \left(\gamma_0 + \frac{p}{p_0} \right), \tag{4.12}$$

where with the values in (4.11), $\theta_p = 4.3$ K. The small coefficient γ_0 is inserted in order that when $p = 0$, the temperature reverts to its value in the absence of an atmosphere, which is 255 K. This corresponds to $\Delta T_p = -33$ K, whence we deduce $\gamma_0 \approx 4.65 \times 10^{-4}$. In practice we can therefore neglect γ_0 , and this we now do (although the term is retained in the numerical code used to solve the model).

It is not easy to estimate the dependence of albedo on ice sheet extent. a must be an increasing function of I . At last glacial maximum, the northern hemisphere ice sheets reached a latitude in North America of some 45° N. A cap of ice cover (sea and land) reaching to this latitude covers 0.15 of the Earth's surface area as opposed to a present day coverage (to 70° N) of 0.03 and if we suppose that the excess fractional cover of 0.12 had an albedo of 0.8 rather than 0.3, then the change of planetary albedo would have been ≈ 0.06 , and multiplying this by $\frac{T}{4(1-a)}$ gives a temperature change of about 6.2 K. Including the enhancement factor due to clouds and water vapour multiplies this by 2.25, suggesting a temperature due to ice cover of $\Delta T_I \approx 13.9$ K. This, however, is an extreme estimate, because sea ice would have had some seasonal variability, and additionally it is likely that the atmosphere would have been less cloudy, thus possibly reducing the enhancement factor (although by its nature it should encompass this possibility). At the opposite extreme, if we suppose that the albedo only changed over the northern ice sheets, of area 2×10^{13} m² and at an average latitude of some 60° N, then the corresponding change of albedo is only 0.01. Multiplication by $\frac{T}{4(1-a)}$ gives a temperature change of 1.03 K, which with enhancement would be 2.3 K.

Combining the two effects of ice and CO₂, we assume that temperature is related to p and I by

$$T - T_0 = \theta_p \ln \left(\gamma_0 + \frac{p}{p_0} \right) - \theta_I I, \tag{4.13}$$

where we take I to be a dimensionless measure of maximum ice extent. Typical values of θ_p and θ_I are given in Table 3, where in general $2 \text{ K} \lesssim \theta_I \lesssim 16 \text{ K}$; we prefer a value of the order of 5 K, since this is an estimate of the actual cooling during the last ice age. We make this equation dimensionless as in (3.51), and this leads to the dimensionless form of the temperature as

$$\theta = \lambda \ln p - \kappa I, \tag{4.14}$$

where we have put $\gamma_0 = 0$, and

$$\lambda = \frac{\theta_p}{\Delta T_c}, \quad \kappa = \frac{\theta_I}{\Delta T_c}. \tag{4.15}$$

Typical values are thus $\lambda \sim 0.33$ and $\kappa \sim 0.38$.

4.2 Nucleation and growth of ice sheets

Our model for ice sheet growth is necessarily a simple one. It is essentially that due to Weertman (1976), and is described in detail below. Similar models have been suggested by, for example, Oerlemans (1980, 1981), MacAyeal (1979), Källén et al. (1979) and Saltzman (2002), and provide for similar bistability.

A cartoon representing Weertman's model is shown in Fig. 5. Weertman considered an ice sheet resting on an isostatically depressed bed. The elevation of the ice above the initial ground surface is h , and the ice depth is then $\frac{3}{2}h$, assuming rock to be three times denser than ice. The northern ice margin is at the (Arctic) ocean, where it forms an ice shelf, and wastage occurs through oceanic melting or iceberg calving. The ice sheet is taken as two-dimensional, with x representing the coordinate southwards from its origin at the northern ice margin. To describe the flow, Weertman assumes plastic flow with a yield stress τ , as a reasonable simplification for the more accurate Glen's law. This being the case, and assuming an active (moving) ice mass, the elevation h satisfies

$$\frac{3}{2}\rho_i g h |h'| = \tau, \tag{4.16}$$

and it follows that if the southern margin is at $x = l$, then

$$h = \{d_i \min(x, l - x)\}^{1/2}, \tag{4.17}$$

where

$$d_i = \frac{4\tau}{3\rho_i g} \approx 4 \text{ m}, \tag{4.18}$$

corresponding to the assumption that $\tau \approx 0.3$ bar. This value is less than Weertman's choice in the range 7–14 m, and is made here to represent the idea that the ice sheet depth $\{d_i l/2\}^{1/2}$ should be of the order of 2,800 m for an ice sheet of extent $l = 4,000$ km. This value is itself intermediate between present day Antarctic depth, and assumed lower elevations of the Laurentide Ice Sheet due to its bed of low yield stress sediments. We take the snowline to be at an elevation $h_0 + sx$ and s is positive.

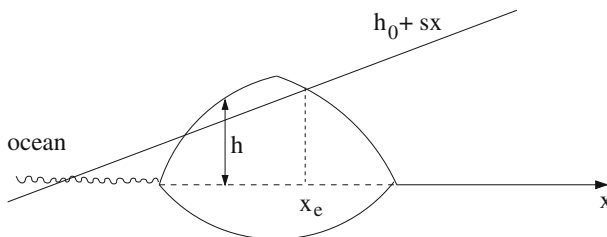


Fig. 5 Cartoon of the growth of the northern hemisphere ice sheets southwards from the Arctic Ocean. The snowline elevation increases towards the south, and divides regions of net accumulation from regions of net ablation

Typically we will suppose $h_0 > 0$. In this case, the ice-free state will be stable, but a finite depth ice sheet can also exist, as indicated in Fig. 5. For the situation shown, where x_e , the value of x where the snowline intersects the ice surface, is on the south-facing slope (i.e., $\frac{1}{2}l < x_e < l$), the rate of change of ice volume in the southern lobe is given by

$$\frac{d}{dt} \int_{\frac{1}{2}l}^l \{d_i(l-x)\}^{1/2} dx = a_i(x_e - \frac{1}{2}l) - m_i(l-x_e), \tag{4.19}$$

in which a_i is mean accumulation rate and m_i is mean melt rate, and x_e is determined by

$$h_0 + sx_e = \{d_i(l-x_e)\}^{1/2}. \tag{4.20}$$

It is convenient to write the resulting ordinary differential equation for l in terms of dimensionless variables, which we initially do by writing

$$l = \frac{d_i L}{s^2}, \quad J = \frac{sh_0}{d_i}, \quad x_e = l(1-\xi), \quad t \sim t_g, \tag{4.21}$$

where we define the ice sheet growth time scale t_g as

$$t_g = \frac{d_i}{sa_i}. \tag{4.22}$$

The ice sheet extent then satisfies the dimensionless equation

$$\dot{L} = \sqrt{2L}[1 - 2(1+\alpha)\xi], \quad 0 < \xi < \frac{1}{2}, \tag{4.23}$$

ξ is given by

$$L\xi + \sqrt{L\xi} = J + L, \tag{4.24}$$

and α by

$$\alpha = \alpha_+ = \frac{m_i}{a_i}. \tag{4.25}$$

We append the suffix ‘+’ because later we will consider α as a variable.

Steady state solutions are given by $L = 0$ (if $J > 0$), and

$$\sqrt{L} = \frac{1}{2}\sqrt{L^*} \left[1 \pm \left\{ 1 - \frac{J}{J^*} \right\}^{1/2} \right], \tag{4.26}$$

where

$$J^* = \frac{\xi^*}{4(1 - \xi^*)}, \quad L^* = \frac{\xi^*}{(1 - \xi^*)^2}, \quad \xi^* = \frac{1}{2(1 + \alpha_+)}; \quad (4.27)$$

it is now natural to finally define

$$L = L^*I, \quad J = J^*H, \quad t_i = t_g\sqrt{L^*}, \quad (4.28)$$

thus

$$l = l_iI, \quad H = \frac{sh_0}{d_iJ^*}, \quad (4.29)$$

where

$$l_i = \frac{d_iL^*}{s^2}, \quad (4.30)$$

and then (4.26) gives the steady states of I as

$$\sqrt{I} = \frac{1}{2} \left[1 \pm \{1 - H\}^{1/2} \right], \quad (4.31)$$

as shown in Fig. 6. The form of the evolution equation for I is described below, following further discussion.

The values of the constants in the ice sheet model, and estimates of their assumed values, are given in Table 4. The solar radiation variation indicated in Fig. 1 represents a 10 % amplitude variation in received solar radiation at 65° N; according to energy balance in (4.8), this corresponds to a surface temperature variation of

$$\Delta T \approx \frac{T\Delta Q_s}{4Q_s} \approx 7.2 \text{ K}, \quad (4.32)$$

Fig. 6 Hysteresis in the steady state ice sheet extent as the elevation of the snowline at the northern margin varies. $I(H)$ is determined by (4.31)

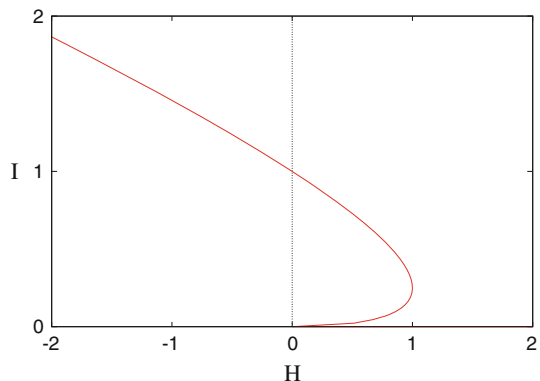


Table 4 Values of additional constants in the ice sheet model

Symbol	Meaning	Typical assumed value
a_i	Mean ice accumulation rate	0.1 m year ⁻¹
d_i	Yield depth	4 m
h_0	Snowline elevation amplitude	1,200 m
H	Elevation parameter	~ 3
l_i	Ice extent scale	3.8×10^3 km
J^*	Scale for J	0.05
L^*	Scale for L	0.24
m_i	Mean ice melt rate	0.2 m year ⁻¹
s	Snowline slope	0.5×10^{-3}
t_i	Ice sheet time scale	40 ka
α_+	Melt rate in advance	2
Γ_A	Atmospheric lapse rate	6 K km ⁻¹
$\Delta Q_s/Q_s$	Milanković variation at 65° N	0.1
ρ_i	Ice density	0.92×10^3 kg m ⁻³

which itself corresponds to a snowline elevation change of 1,200 m, assuming an adiabatic lapse rate of $\Gamma_A = 6 \text{ K km}^{-1}$. We use this as our estimate for h_0 , as it represents the expected Milanković variation in the model.² Weertman uses as an estimate $\alpha_+ = 2.75$, for which we find $\xi^* \approx 0.13$, $J^* \approx 0.04$, $L^* \approx 0.18$. The resulting values of l_i , t_i and H , using the Weertman-based estimate of $\alpha_+ = 2.75$, are $l_i = 2,900$ km and $H \approx 3.75$. If we use an accumulation rate of $a_i = 0.5 \text{ m year}^{-1}$, (Weertman used 1.2 m year^{-1}), we find $t_i = 6$ ka. These values are not that unreasonable, if we associate the time scale with the decay time of ice sheets. Here we choose the slightly different value $\alpha_+ = 2$, which leads to values $\xi^* \approx 0.17$, $J^* = 0.05$ and $L^* = 0.24$, and thus $H = 3$ and $l_i = 3,800$ km. However, it is arguable that although $a_i = 0.5 \text{ m year}^{-1}$ may be appropriate for present day Greenland, it is less likely for the Laurentide, where the accumulation rate may be more desert-like, as for present day Antarctica. If we take an accumulation rate of $a_i = 0.1 \text{ m year}^{-1}$, this gives $t_i = 40,000$ year. (The value for $a_i = 0.5 \text{ m year}^{-1}$ is $t_i = 8,000$ year.)

As shown in Fig. 6, the steady state solution exhibits hysteresis as H varies. The upper and lower branches are stable, and the intermediate one is unstable. Time-dependent evolution of the ice sheet extent is given by (4.23) and (4.24); solving for ξ , we have

$$\xi = 1 + \frac{\frac{1}{2} + J - \left(\frac{1}{4} + J + L\right)^{1/2}}{L}, \tag{4.33}$$

² Note that we have taken Q_s in (4.32) to be the local received radiation, rather than the total given in Table 3. This is because it is the local received radiation which affects the local ground mean temperature, and thus the local snowline elevation, despite the fact that global average temperature is not affected.

and thus the dimensionless volume

$$V_L = \frac{\sqrt{2}}{3} L^{3/2} \tag{4.34}$$

satisfies the equation (with time scaled with t_g)

$$\dot{V}_L = -(1 + 2\alpha)L - 2(1 + \alpha) \left\{ \frac{1}{2} + J - \left(\frac{1}{4} + J + L \right)^{1/2} \right\}. \tag{4.35}$$

Some modification of (4.23) is necessary when $\xi \notin (0, \frac{1}{2})$. In particular, (4.33) makes no sense when L approaches 0, since it implies that $\xi > 1$, whereas its derivation assumes $\xi < \frac{1}{2}$. It is geometrically obvious that for sufficiently large ice sheets, $\xi > \frac{1}{2}$, and the whole southern part of the ice sheet is melting. In this case, the ice is stagnant and we simply put $\xi = \frac{1}{2}$ in (4.23). This is a rough but reasonable approximation since the now dead ice is no longer moving, and the margin is not constrained by the plastic flow assumption.

A similar consideration applies when ξ reaches $\frac{1}{2}$ for small L , providing $J > 0$; at that point the whole ice sheet is below the snowline, and we can again replace ξ by $\frac{1}{2}$. Both cases can be covered by replacing ξ by $\min(\xi, \frac{1}{2})$ if $J > 0$, and thus (4.35) becomes

$$\dot{V}_L = \max \left[(1 + \alpha) \left\{ (1 + 4J + 4L)^{1/2} - (1 + 2J) \right\} - (1 + 2\alpha)L, -\alpha L \right]. \tag{4.36}$$

However, if $J < 0$ and $L = 0$, then an ice sheet will begin to grow spontaneously, i.e., $\dot{L} > 0$. The rate of change of the dimensional volume $\frac{\sqrt{2\lambda}}{3} I^{3/2}$ when $h_0 < 0$ and $l < \frac{-h_0}{s}$ is $\frac{-h_0 a_i}{s}$, and dimensionlessly this leads to

$$\dot{V}_L = -J, \tag{4.37}$$

if $L < -J$, while for $L > -J$, (4.36) still applies. Finally, we can write a uniform definition of \dot{V}_L in the form

$$\dot{V}_L = \max \left[\mathcal{H}(z) \left\{ (1 + \alpha) \left[(1 + 4z)^{1/2} - (1 + 2z) \right] + z \right\} - J, -\alpha L \right], \tag{4.38}$$

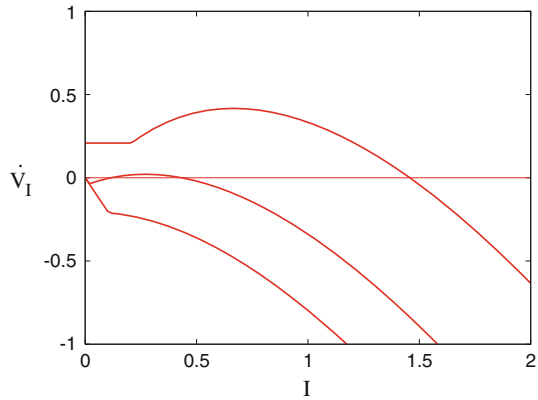
where $\mathcal{H}(z)$ is the Heaviside step function, and $z = J + L$. For the corresponding expression for the dimensionless ice volume

$$V_I = \frac{\sqrt{2}}{3} I^{3/2}, \tag{4.39}$$

we use (4.28), so that, in terms now of the time scale t_i , (4.38) becomes

$$\dot{V}_I = f(I, H, \alpha), \tag{4.40}$$

Fig. 7 The form of \dot{V}_I as a function of I given by (4.40), for values $\alpha = 2$ and $H = -1$ (upper), $H = 0.9$ (middle) and $H = 2$ (lower)



where we define

$$f(I, H, \alpha) = \max \left[\frac{\mathcal{H}(Z) \{ (1 + \alpha) [(1 + 4Z)^{1/2} - (1 + 2Z)] + Z \} - J^* H}{L^*}, -\alpha I \right], \tag{4.41}$$

in which

$$Z = J^* H + L^* I. \tag{4.42}$$

Figure 7 shows the form of \dot{V}_I as a function of I on the three distinct parts of Fig. 6, i.e., where there is only a stable ice sheet, where there is bistability, and where there is no ice sheet. Because J^* and L^* are small (because α is large), we can approximate (4.41) by expanding for small Z , which yields the result

$$\dot{V}_I = \max \left[\mathcal{H}(\zeta) \left\{ \zeta - m^* \zeta^2 \right\} - k^* H, -\alpha I \right], \tag{4.43}$$

where

$$\zeta = I + k^* H, \quad k^* = \frac{1}{4}(1 - \xi^*), \quad m^* = 2L^*(1 + \alpha). \tag{4.44}$$

This can be used instead of (4.40), and it explicitly shows that ice sheet growth occurs on a time scale of t_i .

5 Combined ice and carbon model

Preamble

We now combine the ocean carbon model with the ice sheet model and the energy balance model. This leads to a set of eight dimensionless ordinary differential equations,

together with five constitutive relations. By asymptotic reduction, we show that the model is effectively reduced to just two equations, for ice extent and carbonate ion. The system maintains its hysteretic states, but there are no self sustained oscillations.

5.1 The full dimensionless model

The nonlinear dependence of V_I on I in (4.40) causes an awkwardness in the ice volume equation as $I \rightarrow 0$ which we remove by simply taking $V_I = I$. The combined model is thus, from (3.53), (4.14) and (4.40),

$$\begin{aligned}
 \varepsilon \dot{p} &= 1 - \Omega w - \Lambda(p - p_s), \\
 \eta \dot{Q} &= 2\Lambda(p - p_s) + \Omega w, \\
 v \dot{S} &= -\beta u_b - u_p - \Lambda(p - p_s), \\
 \dot{N} &= \beta u_b + u_p - N, \\
 \zeta \dot{P} &= -u_b + \frac{\gamma \Omega w}{\beta}, \\
 \dot{P}_B &= \frac{\beta u_b}{2\gamma} - P_B, \\
 \omega \dot{I} &= f(I, H, \alpha),
 \end{aligned} \tag{5.1}$$

where $f(I, H, \alpha)$ is given by (4.41), and because the time scale is now $1/B$ rather than t_i , we can define

$$\omega = B t_i; \tag{5.2}$$

for $t_i = 40$ ka, we then have $\omega \sim 0.4$. Additionally, we have the auxiliary functions from (3.54) and (4.14):

$$\begin{aligned}
 \theta &= \lambda \ln p - \kappa I, \\
 p_s &= \frac{Q^2 e^{b\theta}}{S}, \\
 u_b &= (P e^{b'\theta} - 1) P_B, \\
 u_p &= S(1 + \delta_1 Q + \delta_2 S) - \Sigma, \\
 w &= p^\mu e^\theta,
 \end{aligned} \tag{5.3}$$

Before providing numerical solutions of the model, we discuss what we expect to find. Evidently I will tend to a steady state which depends on the parameter H . H was defined in (4.29), and is proportional to h_0 , the snowline elevation in the northern hemisphere at the notional Arctic land-ocean boundary. If $\Gamma_A \sim 6 \text{ K km}^{-1}$ is the adiabatic lapse rate of the atmosphere, then a change of ΔT to the mean atmospheric temperature leads to a change of $\Delta T / \Gamma_A$ to h_0 . In dimensionless terms, the

corresponding change in H due to a change in θ is

$$\Delta H = \phi \Delta \theta, \tag{5.4}$$

where

$$\phi = \frac{s \Delta T_c}{d_i J^* \Gamma_A} \sim 4.1. \tag{5.5}$$

Next, Milanković variation of radiation causes a similar variation in H . We already used the expected local variation of solar radiation Q_s to estimate the corresponding surface temperature change. The corresponding change in H due to a change ΔQ_s to locally received solar radiation Q_s is (cf. (4.32))

$$\Delta H = \psi q_M(t), \tag{5.6}$$

where

$$\psi = \frac{s T_0 \Delta Q_s}{4 d_i J^* Q_s \Gamma_A} \sim 2.3, \tag{5.7}$$

as already found; here $q_M(t)$ is the local received solar radiation Milanković variation at 65° N, normalised to be $O(1)$ in amplitude. Putting these two together, we can write

$$H = H_0 + \phi \theta + \psi q_M, \tag{5.8}$$

where the baseline value H_0 indicates the current interglacial value, which we take to be positive. The values of the dimensionless parameters are given in Table 5.

5.2 The onset of ice ages

The behaviour of the carbon system has been described in Sect. 3. On a 100 year time scale p relaxes to a quasi-equilibrium; on a 5,000 year time scale ocean phosphate equilibrates; then on a 40 ka time scale, carbonate ion S relaxes to a quasi-equilibrium which depends on bicarbonate Q ; finally, on a 300 ka time scale, bicarbonate Q relaxes to its equilibrium in which $\Omega w = 2$. At this point, $N = 1$ and $S \approx 1$, and in pre-glacial times, when we may take $I = 0$, we have

$$Q = \left(\frac{2}{\Omega} \right)^{\frac{1-\lambda b}{2(\lambda+\mu)}}, \tag{5.9}$$

and the temperature is

$$\theta = \frac{\lambda}{\mu + \lambda} \ln \left(\frac{2}{\Omega} \right). \tag{5.10}$$

Table 5 Default values of the dimensionless parameters in the combined ice and carbon model

Symbol	Meaning	Default value
b	Solubility parameter	0.38
b'	Bioproduction parameter	0.9
α	Melt rate	2
β	CaCO ₃ production	3.2
γ	Redfield parameter	0.1
δ_1	Reaction parameter	0.09
δ_2	Reaction parameter	0.023
ε	$p\text{CO}_2$ rate	0.07
η	HCO ₃ ⁻ rate	3.1
ζ	Phosphorus rate	0.05
κ	Ice albedo parameter	0.38
λ	Greenhouse coefficient	0.33
Λ	CO ₂ interfacial transport	70.2
μ	Weathering exponent	0.3
ν	CO ₃ ²⁻ rate	0.4
Σ	Calcite precipitation parameter	0.21
ϕ	Snowline sensitivity	4.1
ψ	Milanković coefficient	2.3
ω	Ice sheet rate	0.4
Ω	Weathering	2

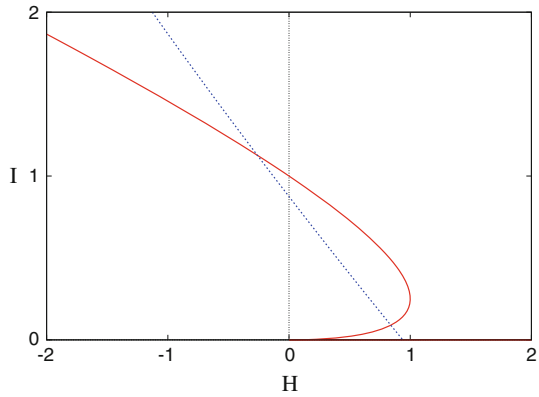
Explicitly, then, we may explain the cooling since the Eocene as being due to a continuous rise in Ω . As stated earlier, this implies either a secular (decreasing) change in volcanism, or an increase of weathering rate, or both, since the Eocene. This explanation requires that weathering continues to increase, presumably associated with mean Himalayan elevation increase. The consequent possible change in ionic concentration L_- apparently has no direct effect on the temperature. Decreasing volcanic production may be associated with decreasing subduction associated with the closure of the Tethys Ocean (Caldeira 1992).

Let us now consider the effect of this slow change of θ on the growth of the Pleistocene ice sheets, ignoring for the moment the effect of Milanković variations. As separate land masses, we can imagine that the growth of the Antarctic Ice sheet at ~ 40 Ma and that of Greenland at ~ 3 Ma followed the same basic pattern.³ Indeed, we can suppose that the present sequence of glacials and interglacials represents a staging post in the formation of a permanent Laurentide Ice Sheet: all due to India!

As θ decreases, so also does H , and when H becomes negative, there is a transition to a permanent ice sheet. However, the resultant cooling lowers the weathering rate, so that there is a consequent feedback on the ice sheet evolution. To understand this,

³ Pollard and DeConto (2005) persuasively suggest that the sudden cooling at 34 Ma is associated with the hysteretic transition from three regional ice caps in Antarctica to a continent wide ice sheet; Antarctic glaciation would thus have been initiated before 34 Ma.

Fig. 8 The nullclines for the $I-S$ system. The $\dot{I} = 0$ nullcline is the graph of (4.31), as shown in Fig. 6, while the $\dot{S} = 0$ nullcline is determined from (5.14) together with (5.12)₃ and (5.8), using $\Omega = 2, \kappa = 0.38, \gamma = 0.2, \mu = 0.3, \Sigma = 0.21, b = 0.38, \lambda = 0.33, \phi = 4.1, \psi = 0$ and $H_0 = 0.5$



we need to understand the dynamics of the coupled $S-I$ system, and this can be done by an understanding of the phase plane, whose behaviour is controlled by the location of the nullclines.

First we consider the dynamics of the carbon system. From (5.1) and (5.3), putting $\varepsilon = \zeta = \delta_1 = \delta_2 = 0$, we derive the equation for S in the form

$$v\dot{S} = (1 - \gamma)\Omega w - S - (1 - \Sigma). \tag{5.11}$$

From the definitions of θ, p and w , we find (allowing $b > 0$)

$$\begin{aligned} \theta &= \frac{\lambda}{1 - \lambda b} \ln \frac{Q^2}{S} - \frac{\kappa}{1 - \lambda b} I, \\ \ln p &= \frac{1}{1 - \lambda b} \ln \frac{Q^2}{S} - \frac{\kappa b}{1 - \lambda b} I, \\ \ln w &= \frac{\mu + \lambda}{1 - \lambda b} \ln \frac{Q^2}{S} - \frac{\kappa(1 + \mu b)}{1 - \lambda b} I. \end{aligned} \tag{5.12}$$

$$\tag{5.13}$$

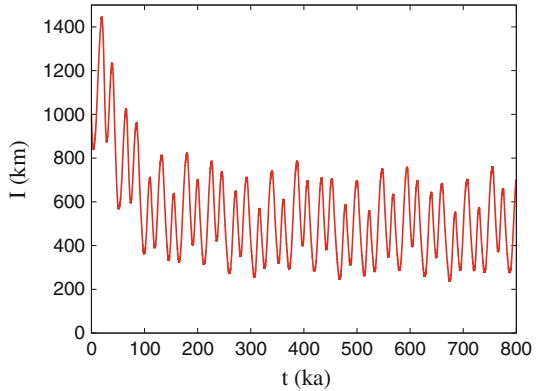
This indicates that S decreases as H increases. Essentially the I nullcline is shown as the equilibrium in Fig. 6, where S increases as H decreases.

To this we need to add the S nullcline, which from (5.11) is found from solving

$$(1 - \gamma)\Omega w = 1 + \Sigma + S. \tag{5.14}$$

Figure 8 shows the nullcline pairs corresponding to the parameter values in Table 5. The figure illustrates the nullclines for $H_0 = 0.5$. The intersection of the nullclines defines three steady states, of which the upper and lower ones are stable, and the intermediate one is unstable, and this is the case for $-0.4 \lesssim H_0 \lesssim 1$. As H_0 increases, the S nullcline moves to the right. For $H_0 \gtrsim 1$, only the ice-free solution exists, and it is stable, while for $H_0 \lesssim -0.4$, the only solution corresponds to a stable permanent ice sheet.

Fig. 9 Solution of the ice sheet growth model with a pseudo-Milanković forcing given by (5.15). Parameters as in the tables, with $h_0 = 200$ m. The initial ice extent is taken as $I = 1,000$ km



The Milanković variation to H is of order $\psi = 2.3$, and thus when $H_0 \sim O(1)$, H will vary back and forth between conditions of stable massive ice sheets and ice-free conditions. If the variation was slow, then we would see oscillatory solutions in which I grows slowly, before H increases and I decreases. If the Milanković variations were slow, then indeed, in this theory, they would drive the sequence of ice ages.

However, the principal fluctuation of solar insolation appears to be too rapid for this to occur. Essentially, the effect of the Milanković variations is to provide a small scale fluctuation about the prevailing steady state. Figure 9 shows the result of forcing the ice sheet/carbon model with a pseudo-Milanković forcing of the form

$$q_M = a_1 \cos \omega_1 t + a_2 \cos \omega_2 t, \tag{5.15}$$

where we choose $a_1 = 0.8$ and $a_2 = 0.4$, and the frequencies ω_1 and ω_2 correspond to periods of 23 and 41 ka. As expected, the solutions are as described above. These may provide a blueprint for the oscillations during the Pliocene, but they do not account for the more recent 100 ka oscillations in the Pleistocene.

Apart from the short period, one feature of this solution which does not resemble the 100 ka oscillations is the observation that recent glacial terminations are rapid. There is nothing as yet in the model which describes this. We might expect this to have a dramatic effect on the dynamics, since when $H \gtrsim 1$, it allows for sudden ice sheet collapse. We now consider this.

6 Proglacial lake formation

Preamble

As Milanković forcing does not produce any kind of realistic oscillations, we now focus on the issue of rapid termination. In order to produce this, we propose that rapid wastage can occur by iceberg calving into proglacial lakes, as suggested by Pollard (1982). We propose a model for the evolution of proglacial lake volume, driven by ice wastage and forefield runoff, and we show that the ice sheet/proglacial lake

model spontaneously oscillates, with a period of the correct order. The carbon cycle is irrelevant to this oscillation.

6.1 Glacial retreat

One of the hallmarks of the oscillations shown in Figs. 1 or 2 is their relaxational sawtooth character. Arguably any model of ice age climate must be able to explain this. In the model as presently written in (4.23), there is nothing to distinguish time scales for growth and decay of ice sheets. We must then ask, what is the physical process which allows ice sheets to grow over a 100 ka time scale, but to completely melt away in 10 ka?

We consider the mechanism to be the following. When an ice sheet is advancing or stationary, the surface meltwater at the margin will flow (on the surface or at the bed via moulins) to the front, where it is able to run off in pro-glacial streams. However, if an ice sheet retreats, then pro-glacial lakes can form in the isostatic depression formed by the ice sheet; and indeed the formation of such lakes is well-known (e.g., Murton et al. 2010). The presence of pro-glacial lakes allows for wastage by calving, and this can allow more rapid shrinkage than plain melting; indeed this is the reason that tide-water glaciers such as Columbia Glacier undergo rapid retreat: a similar mechanism has been postulated as a potential cause for the collapse of the West Antarctic Ice Sheet, and indeed the present rapid retreat of outlet glaciers such as the Pine Island Glacier suggests that this retreat is already under way.

In order to model this dependence of wastage on growth and retreat, we could generalise (4.40) to the form

$$\dot{V}_I = f[I, H, \alpha(\dot{I})], \tag{6.1}$$

where for example

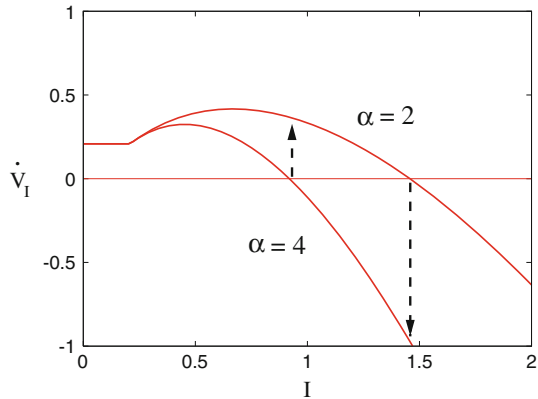
$$\alpha = \alpha_+, \dot{I} \geq 0,$$

$$\alpha = \alpha_-, \dot{I} < 0,$$

and we would choose $\alpha_- > \alpha_+$ to reflect the increased rate of wastage during retreat. More generally, α should be a continuous function which changes rapidly from α_- to α_+ . If the melting time for the ice sheet is about 10 ka, then the melt rate time scale should be about a third of this, and since the time scale for melting is t_i/α_- , this suggests $\alpha_- = 14$ if $t_i = 40$ ka. The consequent value of mean melt rate is $m_- = 1.4$ m year⁻¹ for an accumulation rate of 0.1 m year⁻¹.

A modelling issue now arises. Clearly (6.1) defines \dot{I} implicitly. Equally clearly, it does not define it uniquely if we assume (6.2). For example, Fig. 10 shows \dot{V}_I at $H = -1$ for the two cases in which $\dot{V}_I \geq 0$ and $\dot{V}_I < 0$; clearly, there is a range of values $1 \lesssim I \lesssim 1.5$ where both states are possible. Interestingly, Fig. 10 suggests the possibility of an excitable excursion. If the stable steady state at $I \approx 1.5$ is perturbed through a climatic warming, melting is initiated, \dot{V}_I jumps to the lower state, and I decreases towards $I \approx 1$, where it will jump back to the upper curve, and thus finally

Fig. 10 \dot{V}_I as a function of I for values $H = -1$ and $\alpha = 2$ (upper) and $\alpha = 4$ (lower), representing conditions where $\dot{V}_I \geq 0$ and $\dot{V}_I < 0$, respectively. The arrows indicate a hysteretic transition between the two curves



return to the upper steady state. This is reminiscent of Fig. 1, which we might then interpret as representing a trajectory which continually approaches a steady state at $\delta^{18}\text{O} = 5$, but is frequently excited towards a quasi-steady state at $\delta^{18}\text{O} = 3$.

6.2 The proglacial lake equation

The ambivalence of (6.1) as exhibited by the multiplicity evident in Fig. 10 necessitates the existence of a subsidiary variable which accommodates the transition between the two curves. Evidently this variable can be taken to be proglacial lake volume V_K , and a suitable model for its evolution is

$$\dot{V}_K = l_p m_i l \xi - R_K, \tag{6.2}$$

where the first term on the right is the rate of production of glacial meltwater, and the second is the runoff in proglacial streams. The constant l_p is the ice sheet perimeter, and the dimensionless quantity ξ , introduced in (4.21), must be replaced by 0 if $\xi < 0$, and by $\frac{1}{2}$ if $\xi > \frac{1}{2}$. More specifically, we replace

$$\xi \longrightarrow \min\{\mathcal{H}(Z)\xi, \frac{1}{2}\}, \tag{6.3}$$

where $\mathcal{H}(Z)$ is the Heaviside step function, and Z is defined in (4.42). ξ is defined in (4.33), from which we have

$$L^* I \xi = \frac{1}{2} + Z - (\frac{1}{4} + Z)^{1/2}. \tag{6.4}$$

We make the model dimensionless by writing

$$t \sim \frac{1}{B}, \quad V_K = V_K^0 v, \quad R_K = R_K^0 r \tag{6.5}$$

(note that v is distinct from its earlier usage as the volcanic carbon input), whence we have

$$\delta \dot{v} = M^* \Xi(I, H) \alpha(v) - r(v), \tag{6.6}$$

where we define

$$\Xi = \frac{I}{L^*} \min\{\mathcal{H}(Z)\xi, \frac{1}{2}\}, \tag{6.7}$$

and the parameters are defined by

$$\delta = \frac{BV_K^0}{R_K^0}, \quad M^* = \frac{l_p a_i d_i L^{*2}}{s^2 R_K^0}. \tag{6.8}$$

We have assumed that the melt rate m_i is an (increasing) function of lake volume, so that α is a function of v .

In the normal case where $0 < \xi < \frac{1}{2}$, we can approximate Ξ by expanding (6.4) for small Z . The result is

$$\Xi \approx (I + k^* H)^2, \tag{6.9}$$

where $k^* = \frac{J^*}{L^*}$ was defined in (4.44); this explains the reason for including L^* in the definition of Ξ . More generally,

$$\Xi \approx I \min \left[\mathcal{H}(I + k^* H) \frac{(I + k^* H)^2}{I}, \frac{1}{2L^*} \right], \tag{6.10}$$

and is a non-negative increasing function of I .

To estimate the parameters, we conceive of a stream network spaced at intervals of 20 km (based on typical Laurentide or Fennoscandian esker spacing, Boulton et al. 2009; Shreve 1985) having discharges of $50 \text{ m}^3 \text{ s}^{-1}$ (Wingham et al. 2006). Over an assumed perimeter of $l_p = 4,000 \text{ km}$, this yields $R_K^0 = 3 \times 10^{11} \text{ m}^3 \text{ year}^{-1}$. The proglacial lake volume is taken to be a value representative of the high stand of Lake Agassiz during the last ice age (Leverington et al. 2000), thus $V_K^0 = 20,000 \text{ km}^3$. With these choices, we find $M^* \approx 1.23$, $\delta \approx 0.7 \times 10^{-3}$. It is not surprising that $M^* = O(1)$, since in a steady state melt and runoff must balance. Table 6 gives the typical values of the dimensional and dimensionless parameters introduced in the present section.

As mentioned, we suppose $\alpha = \alpha_+$ when $v = 0$. Although calving rates are not well constrained, it seems that they increase with water depth (Cuffey and Paterson 2010, p. 123), so that we suppose that α is an increasing function of v . On the other hand, runoff r is largely determined by the geometry of the outlet stream systems. We expect it to increase as v increases, due to the occurrence of new ‘overflow’ points. However, we also expect that there will be some threshold value, where flooding occurs and the lake drains to the sea (Murton et al. 2010), and we identify this with the value of V_K^0 .

Table 6 Values of additional constants in the proglacial lake model

Symbol	Meaning	Typical assumed value
l_p	Ice sheet perimeter	4,000 km
m_-	Ice wastage rate in retreat	2 m year ⁻¹
M^*	Melt rate parameter	1.27
R_K^0	Proglacial stream runoff	3×10^{11} m ³ year ⁻¹
V_K^0	Proglacial lake volume	20,000 km ³
α_-	Melt rate in retreat	20
δ	Proglacial lake filling parameter	0.7×10^{-3}

In addition, the rise in sea level of 120 m in 10,000 years at the last glacial termination suggests a meltwater flux of 4.3×10^{12} m³ year⁻¹, some 14 times larger than our normal glacial runoff scale. We choose our runoff and melt functions to allow for this possibility.

It is clear that, depending on the choice of α and r , hysteresis can occur, as shown in Fig. 11. In practice $\dot{v}(0) < 0$ at sufficiently low Σ , so that in that case the lake drains to zero volume in finite time. It is numerically convenient to alter the behaviour at $v = 0$ so that $\dot{v} = 0$ there, and we do this in Fig. 11 by multiplying the right-hand side of (6.6), let us say g , by $1 - \{1 - \mathcal{H}(g)\} \exp\{-100v\}$, where \mathcal{H} is the Heaviside step function. The expressions for α and r are taken as

$$\alpha = \alpha_- - (\alpha_- - \alpha_+)e^{-4v}, \quad r = \exp\left[\frac{0.03}{1-v}\right]. \tag{6.11}$$

Figure 12 shows the solutions for ice extent and lake volume corresponding to the same parameter values used in Fig. 9, except that we remove the Milanković forcing, $q_M = 0$. We take $m_- = 2$ m year⁻¹, so that $\alpha_- = 20$. Self-sustained oscillations occur, and these now have an appropriate sawtooth character, as well as a long period unrelated to any forcing (of which there is none).

Fig. 11 Plots of (6.6) for parameters $M^* = 1$ and $\Xi = 0.1, 0.3$ and 1, representing conditions of increasing ice volume. The assumed forms for α and r are given in (6.11), with $\alpha_- = 4, \alpha_+ = 2$. In order to accommodate $\dot{v} \geq 0$ at $v = 0$, the right-hand side of (6.11) has been multiplied by $1 - \{1 - \mathcal{H}(\dot{v})\} \exp\{-100v\}$, where $\mathcal{H}(\cdot)$ is the Heaviside step function

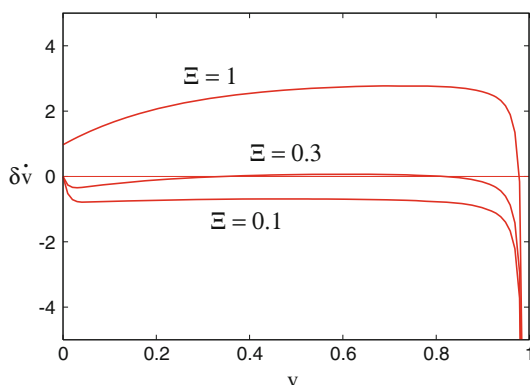
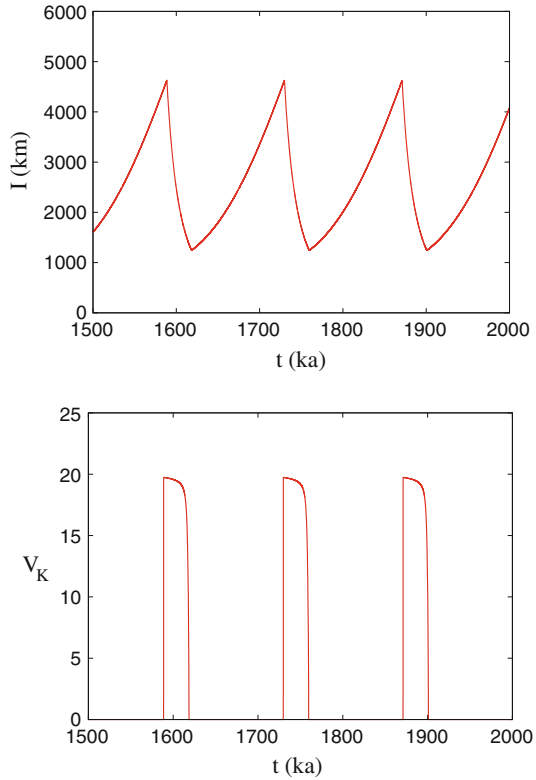


Fig. 12 Numerical solution of the combined ice/carbon/lake model using the parameter values in the tables, except that $h_0 = 400$ m (also $b_3 = 0$)



The mechanism of these oscillations is fairly readily explained with reference to Figs. 8 and 11. Essentially, we take $\alpha = \alpha_+$ if $v = 0$ and $\alpha = \alpha_-$ if $v > 0$. From Fig. 11, we have that $v > 0$, thus $\alpha = \alpha_-$ if $\Xi > \Xi_+$, where

$$\Xi_+ = \frac{1}{M^* \alpha_+}, \tag{6.12}$$

while $v = 0$ for $\Xi < \Xi_-$, where

$$\Xi_- = \frac{1}{M^* \alpha_-}; \tag{6.13}$$

between these two values, either state is possible. Figure 13 indicates the resultant dynamics. The blue (online) curve labelled S is the S nullcline, the red (online) curve labelled I is the I nullcline when $v = 0$, i.e., $\alpha = \alpha_+$; the green (online) curve labelled S_- is the corresponding nullcline for $v > 0$, when $\alpha = \alpha_-$: it (the green curve) is given by

$$\sqrt{I} = \frac{1}{2} \sqrt{I_-} \left[1 \pm \left(1 - \frac{H}{j_-} \right)^{1/2} \right], \tag{6.14}$$

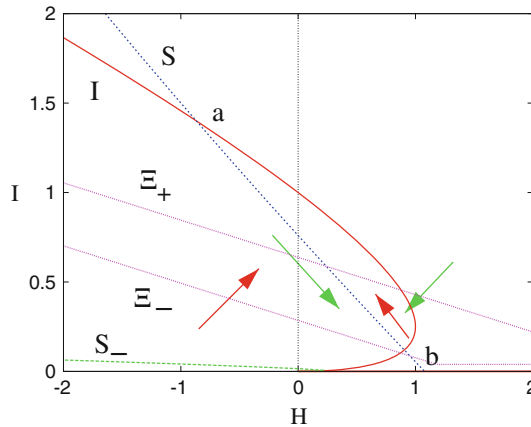


Fig. 13 Effect of lake volume hysteresis on ice sheet dynamics. Trajectories below the *lower lilac curve* labelled ξ_- move upwards, as indicated by the *red arrows*, until they reach the *upper lilac curve*, labelled ξ_+ , at which point they switch to the downwards moving branch of trajectories, indicated by the *green arrows*. Conversely, trajectories above ξ_+ move downwards (*green arrows*) until they reach ξ_- , when they switch to the up (*red*) trajectories. The up trajectories are approaching the (inaccessible) fixed point at (a), while the down trajectories are approaching the fixed point at (b). In this way a self-sustaining oscillation is maintained (colour figure online)

where

$$j_- = \frac{1 + 2\alpha_+}{1 + 2\alpha_-}, \quad l_- = \left(\frac{1 + \alpha_-}{1 + \alpha_+} \right) j_-^2; \tag{6.15}$$

we use values $\alpha_+ = 2, \alpha_- = 10$, for which $j_- = 0.24, l_- = 0.015$. For $v = 0$, trajectories migrate upwards towards the ice sheet state, but then reach a threshold where lake volume increases, and trajectories switch to the green (downward) ones trying to reach the ice-free state. In this way the self-sustaining oscillation is maintained.

7 Rapid CO₂ rise

Preamble

The necessity to have a model in which glacial terminations occur rapidly has led us to propose an explicit model for proglacial lake growth, and this now produces ice sheet oscillations of the desired form. However, we have come a long way from our starting point, which was the idea that carbon was likely to be a driver for ice ages. Now we find that, because carbon is coupled to the ice sheet model, it also oscillates, but the oscillations are completely unlike the observations. Therefore we need to find a mechanism which can explain the rapid CO₂ rise, and this section examines various possibilities in turn.

The first is the dilution effect, whereby raising of sea level at terminations causes a decrease in ocean salinity. Because the negative conservative ion concentration L_- of

17.4 mM is about seventy times larger than the CO_2 controlling carbonate concentration of 0.24 mM, it seems plausible that small changes in L_- could have a significant effect; but we find that change in ocean volume is insufficient to support the change.

Next, we consider the effects of altered weathering rates by consideration of a much more detailed discussion of weathering, involving dissolution of silicate, carbonate and feldspar, as well as other species. This eventually leads to a modified carbonate ion equation in which the weathering coefficient Ω (now written as one of several, Ω_S) depends on ice volume through sea level induced exposure of continental shelf carbonates. However, there is still no mechanism to induce rapid CO_2 rise on termination.

Finally, we realise that the key is to find an ingredient of the model with a built in rapid time scale, and this ingredient is phosphorus and thus biomass; and the mechanism which is able to induce the necessary rapid rise is the temperature dependence of biomass growth.

7.1 Continental shelf exposure

It is clear from Fig. 2 that p_{CO_2} follows $\delta^{18}\text{O}$ relatively closely. In the model, at least at the moment, this is not the case. The temperature oscillates in a way fairly similar to the ice, but the oscillation of CO_2 is much more regular. This is because, according to (5.12)₂, $p \sim \frac{1}{S}$, and according to (5.11) (given the definition of w in (5.12)₃), S changes on a time scale of $O(1)$. Worse, since the equilibrium of (5.11) has S as a decreasing function of I , it follows that as I increases during an ice age, S decreases and thus p increases, in stark contrast to the data.

Something is missing from the model. One effect of the growth of continental ice sheets is that the sea level drops. In the last ice age, sea level was 120 m lower, and thus large areas of continental shelf were exposed. There are several consequences of this, all of which might seem to provide some relevant modification to the model.

Firstly, a significant portion of the marine biomass which acts as the agent for calcium and carbonate extraction and burial is removed. This suggests that the burial coefficient B may reasonably be taken as a decreasing function of I . Secondly, the exposure of the carbonate-rich sediments of the shelves is liable to increase the rate of physical weathering, which would suggest that W_0 , and thus also Ω , should be an increasing function of ice extent I . Finally, the decrease in ocean volume leads to a change in the concentration of the ionic species. Because the volume change is relatively small, so also are the concentration changes, but the effect is important in its alteration of the conservative negative ion, because this has a concentration much greater than the CO_2 -controlling carbonate ion.

Because burial does not directly affect the carbonate ion, variation of B will not have much effect on the results. If the physical weathering rate parameter Ω increases sufficiently rapidly with I , then we can see from (5.12) that the equilibrium S of (5.11) will be an increasing function of I , which can potentially alleviate the incorrect phasing of CO_2 with ice volume.

However, what is crucial is that the CO_2 should change rapidly with ice volume at termination. The direct physical effect which might cause this is the re-dilution of

the world's ocean, and this suggests that it could be the third effect alluded to above which is the missing essential ingredient. We now reconsider the ocean chemistry model, except that now we allow for the variation in ocean volume V_{oc} .

In dimensional terms, ocean volume is determined by

$$\rho_w V_{oc} + \rho_i V_I = \rho_w V_{oc}^0, \tag{7.1}$$

where V_I is ice sheet volume, and V_{oc}^0 is a reference value. Conservation of negative conservative ionic species is therefore prescribed by

$$L_- V_{oc} = L_-^0 V_{oc}^0, \tag{7.2}$$

and thus

$$L_- = L_-^0 \left(1 - \frac{\rho_i V_I}{\rho_w V_{oc}^0} \right)^{-1} \approx L_-^0 + \frac{\rho_i V_I L_-^0}{\rho_w V_{oc}^0}, \tag{7.3}$$

since the change of ocean volume is relatively small. Note that (cf. (4.19)) the ice volume is given by

$$V_I = 2l_p \int_{1/2l}^l \{d_i(l-x)\}^{1/2} dx, \tag{7.4}$$

and thus

$$V_I = V_I^0 V_I^*, \tag{7.5}$$

where we define

$$V_I^0 = d_i^{1/2} l_p l_i^{3/2} \tag{7.6}$$

and (cf. (4.39))

$$V_I^* = \frac{\sqrt{2}}{3} I^{3/2}. \tag{7.7}$$

We then have

$$L_- \approx L_-^0 + \delta_3 L_-^0 V_I^*, \tag{7.8}$$

where

$$\delta_3 = \frac{\rho_i V_I^0}{\rho_w V_{oc}^0}. \tag{7.9}$$

The ocean equations in (3.40) are modified, allowing for the variation of V_{oc} as above, to

$$\begin{aligned}
 (V_{oc}\dot{C}) &= V_{oc}[h(p - p_s) + A^*W - R_3 - R_4], \\
 (V_{oc}\dot{Z}) &= V_{oc}[\frac{1}{2}A^*W - R_3 - R_4], \\
 (V_{oc}\dot{N}) &= V_{oc}[R_3 + R_4 - BN], \\
 R(V_{oc}\dot{P}) &= V_{oc}[-R_3 + \rho RA^*W], \\
 R(V_{oc}\dot{P}_B) &= V_{oc}[R_3 - BRP_B],
 \end{aligned}
 \tag{7.10}$$

and using (7.8), these can be written in the form

$$\begin{aligned}
 \dot{C} &\approx r_i \dot{V}_I C + h(p - p_s) + A^*W - R_3 - R_4, \\
 \dot{Z} &\approx r_i \dot{V}_I Z + \frac{1}{2}A^*W - R_3 - R_4, \\
 \dot{N} &\approx r_i \dot{V}_I N + R_3 + R_4 - BN, \\
 R\dot{P} &\approx r_i \dot{V}_I P - R_3 + \rho RA^*W, \\
 R\dot{P}_B &\approx r_i \dot{V}_I P_B + R_3 - BRP_B,
 \end{aligned}
 \tag{7.11}$$

where

$$r_i = \frac{\rho_i}{\rho_w V_{oc}^0}.
 \tag{7.12}$$

The equations for C and Z are replaced by those for Q and S , defined as in (3.41) by

$$Q = L_- + 2C - 2Z, \quad S = 2Z - L_- - C.
 \tag{7.13}$$

Using (7.3), this leads, after some algebra, to the two modified equations for Q and S in the form

$$\begin{aligned}
 \dot{Q} &= r_i \left[Q - r_i L_-^0 V_I \right] \dot{V}_I + 2h(p - p_s) + A^*W, \\
 \dot{S} &= r_i \left[S + r_i L_-^0 V_I \right] \dot{V}_I - h(p - p_s) - R_3 - R_4.
 \end{aligned}
 \tag{7.14}$$

These differ from those in (3.50) by the presence of the terms in \dot{V}_I , and it is precisely these terms which might allow rapid change in S and Q during deglaciation. We can see from (7.14) that as V_I decreases, S does as well, allowing for p_{CO_2} to rise; although we have yet to ascertain whether the effect is significant.

The equations are non-dimensionalised as in (3.51) and (7.5), and this leads to the modification to (3.53) as

$$\begin{aligned}
 \eta \dot{Q} &= \chi \omega [\delta_1 Q - \delta_3 V_I^*] \dot{V}_I^* + 2\Lambda(p - p_s) + \Omega w, \\
 \nu \dot{S} &= \chi \omega \left[\frac{1}{2} \delta_2 S + \delta_3 V_I^* \right] \dot{V}_I^* - \beta u_b - u_p - \Lambda(p - p_s), \\
 \dot{N} - \delta_3 \dot{V}_I^* N &= \beta u_b + u_p - N, \\
 \zeta (\dot{P} - \delta_3 \dot{V}_I^* P) &= -u_b + \frac{\gamma \Omega w}{\beta}, \\
 2\gamma (\dot{P}_B - \delta_3 \dot{V}_I^* P_B) &= \beta u_b - 2\gamma P_B,
 \end{aligned}
 \tag{7.15}$$

where δ_3 was defined in (7.9), and

$$\chi = \frac{\rho_i V_I^0 L_-^0}{\rho_w V_{oc}^0 v t_i}.
 \tag{7.16}$$

Using the values in Tables 1, 2 and 3, we find

$$\delta_3 \approx 0.041, \quad \chi \approx 3.55.
 \tag{7.17}$$

The values of other extra parameters introduced are given in Table 7.

Analysis of the dilution model

Now we analyse how the solutions of this model should behave. As before, on a time scale $t \sim \varepsilon$, p relaxes to equilibrium,

$$\Lambda(p - p_s) = 1 - \Omega w,
 \tag{7.18}$$

while on a time scale $t \sim \zeta$, P relaxes to the approximate equilibrium

$$\beta u_b = \gamma \Omega w,
 \tag{7.19}$$

Table 7 Values of additional constants in the ocean dilution model

Symbol	Meaning	Typical assumed value
L_-^0	Negative conservative ions	17.4 mM
V_I^0	Ice sheet volume scale	$0.6 \times 10^{17} \text{ m}^3$
V_{oc}^0	Ocean volume scale	$1.35 \times 10^{18} \text{ m}^3$
δ_3	Ice volume parameter	0.041
ρ_w	Water density	10^3 kg m^{-3}
χ	Ocean dilution	3.55

while also

$$u_p \approx S - \Sigma. \tag{7.20}$$

Q varies on the longer time scale $t \sim \eta$, and thus is relatively constant. The effective model to be solved thus consists of the equations for carbonate ion, ice sheet extent and proglacial lake volume:

$$\begin{aligned} v\dot{S} &= (1 - \gamma)\Omega w - (1 - \Sigma + S) + \chi \left[\frac{1}{2}\delta_2 S + \delta_3 I \right] f, \\ \omega\dot{I} &= f[I, H, \alpha(v)], \\ \delta\dot{v} &= M^* \Xi \alpha(v) - r(v), \end{aligned} \tag{7.21}$$

where, as in (5.1), we have identified $\dot{V}_I = \dot{I}$, and (4.41) defines $f(I, H, \alpha)$. In practice, we also have (6.9):

$$\Xi \approx (I + k^* H)^2, \tag{7.22}$$

and the approximation of (4.43) to allow for variable α is, over most of the range of I ,

$$f \approx I - m^*(I + k^* H)^2, \tag{7.23}$$

where

$$m^* = \frac{(\alpha_+ + 1)\{1 + \alpha(v)\}}{(\alpha_+ + \frac{1}{2})^2}. \tag{7.24}$$

Let us suppose that initially $v = 0$ and we take $H < 1$, essentially as in Fig. 13. I grows on a time scale $t \sim \omega$ towards an equilibrium at

$$I = I_+ \approx \frac{1}{m^*_+}, \quad m^*_+ = \left(\frac{\alpha_+ + 1}{\alpha_+ + \frac{1}{2}} \right)^2 = O(1). \tag{7.25}$$

Since $\chi\delta_3$ is small, the S nullcline in Fig. 13 is only shifted a little. As I grows, Ξ increases; when Ξ reaches Ξ_+ , where

$$\Xi_+ = \frac{1}{M^* \alpha_+}, \tag{7.26}$$

then v jumps rapidly to a positive equilibrium where $\alpha = \alpha_-$, and f jumps to the value

$$f \approx I - m^*_-(I + k^* H)^2, \tag{7.27}$$

where

$$m_-^* = \frac{(\alpha_+ + 1)(\alpha_- + 1)}{(\alpha_+ + \frac{1}{2})^2} \sim \frac{\alpha_-}{\alpha_+} \gg 1. \tag{7.28}$$

Thus in this termination phase, I decreases on a time scale $t \sim \frac{\omega}{m_-^*} \ll 1$, until v drops to zero again, which is when $\Xi \approx \Xi_-$, where

$$\Xi_- = \frac{1}{M^* \alpha_-}. \tag{7.29}$$

The carbonate ion is a fairly passive player in this, but we can see from (7.21)₁ that if the termination time scale $t \sim \frac{\omega}{m_-^*}$ is sufficiently short, then

$$v\dot{S} \approx \chi\omega \left[\frac{1}{2}\delta_2 S + \delta_3 I \right] \dot{I}. \tag{7.30}$$

The variation of S with I can be solved exactly, but since δ_2 and δ_3 are small, we have directly

$$S \approx S_+ + \delta_3 S_+ I + \frac{\delta_3^2}{\delta_2} I^2, \tag{7.31}$$

and similarly

$$Q \approx Q_+ + \delta_3 Q_+ I - \frac{\delta_3^2}{2\delta_1} I^2, \tag{7.32}$$

where Q_+ and S_+ are constants, and we use the fact that

$$\delta_3 = \frac{\chi\omega\delta_1}{\eta} = \frac{\chi\omega\delta_2}{2\nu}. \tag{7.33}$$

The potential for a rapid drawdown of carbonate ion lies in the quadratic term in (7.32), since although the volume change parameter δ_3 is small, the small reaction parameter δ_2 is also. Unfortunately, the values in Table 5 indicate that the latter is not small enough. The combined effect of the changes in Q and S lead to a relative rise in $p\text{CO}_2$ of about 0.05, corresponding to about 9 ppmv, about a tenth of what is observed. These results suggest that the variation in ocean volume is not a significant effect, and we therefore henceforth ignore it.

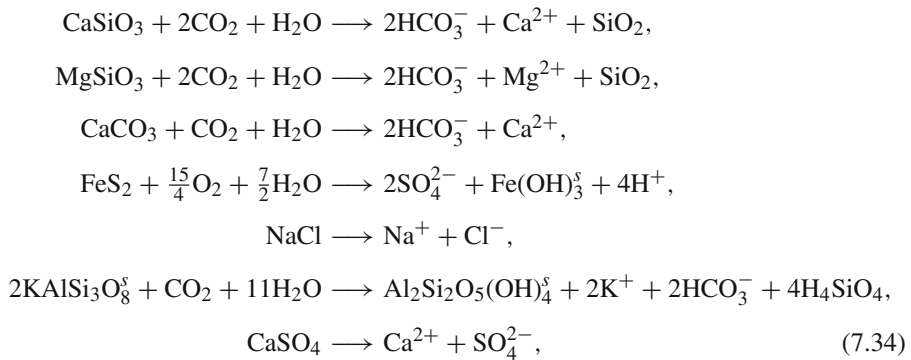
7.2 River chemistry

Since the ocean dilution effect is not large enough to produce the necessary jump down in carbonate ion at termination, we must consider other possibilities. One clue

as to where to look comes from an inspection of river chemistry. Measurement of ionic concentration in rivers (e.g., Emerson and Hedges 2008, table 2.1) shows that the source term of conservative ions to the ocean is such that far from our assumption that $\dot{L}_- = 0$, which follows from (3.30)₂, L_- is presently decreasing in such a way that it would reach $L_- = 0$ in 3.5 My. It is generally thought that variation of these conservative ions occurs, if at all, on a much longer time scale, and it seems unlikely that this rate of decrease is anything other than temporary.

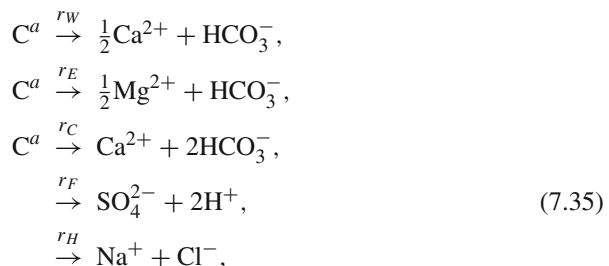
The implication of this is that the rate of weathering changes as the ice sheets grow, in such a way that $\dot{L}_- > 0$ during ice ages, with a mean rate of change of zero. We therefore return to a more detailed discussion of weathering. While the reactions (3.5) and (3.10) do indeed occur, they carry the latent and incorrect implication that L_- is constant. To allow for a more complete discussion, we must consider ways in which the other conservative ions are produced.

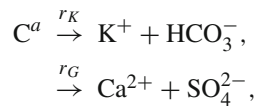
Of course there are many other weathering reactions which involve carbon but not calcium; for example the pyroxenes replace Ca in (3.5) with Mg or Na or other ions. We now consider an elaborated set of weathering reactions given by



which represent respectively weathering of wollastonite, enstatite (Mg replaces Ca) and carbonate; oxidation of pyrite, dissolution of halite, formation of kaolinite from K-feldspar, and dissolution of gypsum. There are many other reactions one could add, and we do not mean to imply that these are the most important, but they will serve the purpose of our discussion.

The essence of the reactions is given by





in which C^a denotes atmospheric carbon, and the coefficients r_j denote the reaction rates. The left-hand sides of the fourth, fifth and seventh reactions are empty because no atmospheric carbon is used in them. These reactions then provide the source terms for the oceanic concentrations of the ionic species, in the form

$$\begin{aligned}
 [HCO_3^-] &= r_W + r_E + 2r_C + r_K, \\
 [H^+] &= 2r_F, \\
 [Ca^{2+}] &= \frac{1}{2}r_W + r_C + r_G, \\
 [Mg^{2+}] &= \frac{1}{2}r_E, \\
 [Na^+] &= r_H, \\
 [K^+] &= r_K, \\
 [SO_4^{2-}] &= r_F + r_G, \\
 [Cl^-] &= r_H, \\
 [CO_2^a] &= -(r_W + r_E + r_C + r_K),
 \end{aligned} \tag{7.36}$$

where the units of the concentrations are M. These source terms must be added to the other terms in (3.24), and very small removal terms representing precipitation of the conservative ions can be included, but are ignored here. Denoting L_- by (3.1) and L_+ by (3.29), it follows that

$$\dot{L}_- = 2r_F + 2r_G - r_E - r_K, \tag{7.37}$$

and is no longer necessarily constant.

Values of these rate constants can be estimated from the observed concentrations of river ion concentrations, as given for example by Emerson and Hedges (2008, table 2.1) or Krauskopf and Bird (1995, table 12.4). It should be borne in mind that these estimates are based on the particular set of reactions which are considered. The estimates use the fact that the source of an ion of river concentration c_i (units M) to the ocean is $c_i r_{oc}$, where $r_{oc} = 3.5 \times 10^{13} \text{ m}^3 \text{ year}^{-1}$ is the net river flow to the oceans. This gives the source in units of $\text{M m}^3 \text{ year}^{-1}$, and to convert to M year^{-1} , (as in (7.36)), we divide by the ocean volume V_{oc} . Defining oceanic residence time

$$t_{oc} = \frac{V_{oc}}{r_{oc}} = 0.39 \times 10^5 \text{ year}, \tag{7.38}$$

(7.36) leads to the estimates

$$\begin{aligned}
 t_{oc}[r_W + r_E + 2r_C + r_K] &= c_{\text{HCO}_3^-}, \\
 t_{oc}[r_F + r_G] &= c_{\text{SO}_4^{2-}}, \\
 t_{oc}r_H &= c_{\text{Cl}^-}, \\
 t_{oc}[r_C + \frac{1}{2}r_W + r_G] &= c_{\text{Ca}^{2+}}, \\
 t_{oc}r_E &= c_{\text{Mg}^{2+}}, \\
 t_{oc}r_H &= c_{\text{Na}^+}, \\
 t_{oc}r_K &= c_{\text{K}^+},
 \end{aligned}
 \tag{7.39}$$

from which we can also deduce

$$\begin{aligned}
 t_{oc}[r_C + \frac{1}{2}r_W] &= \frac{1}{2} \left(c_{\text{HCO}_3^-} - c_{\text{Mg}^{2+}} - c_{\text{K}^+} \right), \\
 t_{oc}r_G &= c_{\text{Ca}^{2+}} - \frac{1}{2} \left(c_{\text{HCO}_3^-} - c_{\text{Mg}^{2+}} - c_{\text{K}^+} \right), \\
 t_{oc}r_F &= c_{\text{SO}_4^{2-}} - c_{\text{Ca}^{2+}} + \frac{1}{2} \left(c_{\text{HCO}_3^-} - c_{\text{Mg}^{2+}} - c_{\text{K}^+} \right).
 \end{aligned}
 \tag{7.40}$$

Note that consistency in (7.39) requires $c_{\text{Na}^+} = c_{\text{Cl}^-}$, which is not exactly true. Of course this is because Na^+ is produced by other reactions, whose inclusion would allow such consistency. Our purpose is not to try and make these reaction rates precise, and so we will tolerate this slight inconsistency. Values of the river concentrations are given in Table 8, together with the derived estimates for the reaction rates.

The equations equivalent to (3.24) are now

$$\begin{aligned}
 [\dot{\text{CO}}_2] &= -R_1 + h(p - p_s), \\
 [\dot{\text{CO}}_3^{2-}] &= R_2 - R_4, \\
 [\dot{\text{HCO}}_3^-] &= R_1 - R_2 - R_3 + r_E + r_K + 2r_C + r_W, \\
 [\dot{\text{H}}^+] &= R_1 + R_2 + R_3 + 2r_F, \\
 [\dot{\text{Ca}}^{2+}] &= -R_3 - R_4 + r_C + \frac{1}{2}r_W + r_G, \\
 [\dot{\text{CaCO}}_3] &= R_3 + R_4 - B[\text{CaCO}_3], \\
 [\dot{\text{P}}] &= -R_3 + Rr_P, \\
 [\dot{\text{P}}_B] &= R_3 - B[\text{P}_B],
 \end{aligned}
 \tag{7.41}$$

where r_P is the supply rate of phosphorus, determined in Table 8 by means of the average river concentration. In addition (7.37) determines L_- .

The only thing that now changes in the simplification of the model is that the reactive source terms are slightly different; other than that, the discussion proceeds as

Table 8 Values of world average river and glacial stream concentrations and the consequent reaction rates of (7.35)

Symbol	Meaning	River	Glacial	Ocean
$c_{\text{HCO}_3^-}$	Bicarbonate	0.96	0.85	2.0
$c_{\text{SO}_4^{2-}}$	Sulphate	0.11	0.08	28.2
c_{Cl^-}	Chloride	0.22	0.16	545.9
$c_{\text{Ca}^{2+}}$	Calcium	0.37	0.34	10.3
$c_{\text{Mg}^{2+}}$	Magnesium	0.17	0.14	52.8
c_{Na^+}	Sodium	0.26	0.22	469.1
c_{K^+}	Potassium	0.07	0.03	10.2
c_P	Phosphorus	1.3×10^{-3}	$\sim 3 \times 10^{-3}$	2.2×10^{-3}
$t_{oc}r_H$	Halite rate	0.22–0.26	0.16–0.22	
$t_{oc}r_E$	Enstatite rate	0.17	0.14	
$t_{oc}r_K$	K-feldspar rate	0.07	0.03	
$t_{oc} \left[r_C + \frac{1}{2}r_W \right]$	Carbonate/wollastonite rate	0.27	0.34	
$t_{oc}r_G$	Gypsum rate	0.105	0	
$t_{oc}r_F$	Pyrite rate	0.01	0.08	
$t_{oc}r_P$	Phosphorus rate	1.3×10^{-3}	1.3×10^{-3}	

Also given are the oceanic concentrations. All units are in mM. River and ocean values from Emerson and Hedges (2008), glacial values from Tranter (2006). P data from Jahnke (1992) and Hodson (2006)

before. From (7.37) and (7.41), we have

$$\begin{aligned}
 \dot{L}_- &= 2r_F + 2r_G - r_E - r_K, \\
 \dot{C} &= h(p - p_s) - R_3 - R_4 + r_E + r_K + 2r_C + r_W, \\
 \dot{Z} &= -R_3 - R_4 + r_C + \frac{1}{2}r_W + r_G,
 \end{aligned}
 \tag{7.42}$$

and thus from (3.36),

$$\begin{aligned}
 \dot{Q} &= 2h(p - p_s) + 2r_F + 2r_C + r_E + r_K + r_W, \\
 \dot{S} &= -h(p - p_s) - R_3 - R_4 - 2r_F.
 \end{aligned}
 \tag{7.43}$$

Equivalently, the atmospheric CO₂ equation is, following (3.50),

$$\frac{A_E}{M_a g m_{oc}} \dot{p} = v - h(p - p_s) - (r_W + r_E + r_C + r_K),
 \tag{7.44}$$

Non-dimensionalisation proceeds as in (3.51). The reaction rates r_j will generally have different temperature and p_{CO_2} dependences, but we assume they are all proportional to the weathering function w . We define concentrations c_Q, c_A, c_S, c_-, c_+ and

c_P by the relations

$$\begin{aligned}
 t_{oc}[r_W + r_E + r_K - 2r_F] &= c_Q w, \\
 t_{oc}[r_W + r_E + r_K + r_C] &= c_A w, \\
 t_{oc}[r_W + r_E + r_K + r_C - 2r_F] &= c_S w, \\
 2t_{oc}[r_F + r_G] &= c_- w, \\
 t_{oc}[r_E + r_K] &= c_+ w, \\
 t_{oc}r_P &= c_P w,
 \end{aligned}
 \tag{7.45}$$

and note from the values in Table 8 that present day estimates are, taking $w = 1$,

$$\begin{aligned}
 c_Q &\sim 0.58, & c_A &\sim 0.78, & c_S &\sim 0.76, \\
 c_- &\sim 0.23, & c_+ &\sim 0.42, & c_P &\sim 1.3 \times 10^{-3},
 \end{aligned}
 \tag{7.46}$$

with units being mM, and assuming arbitrarily that $r_C = r_W$.

The non-dimensional equations which are modified from those in (3.53) are

$$\begin{aligned}
 \varepsilon \dot{p} &= 1 - \Lambda(p - p_s) - \Omega_A w, \\
 \eta \dot{Q} &= 2\Lambda(p - p_s) + (2\Omega_A - \Omega_Q)w, \\
 \nu \dot{S} &= -\beta u_b - u_p - \Lambda(p - p_s) - (\Omega_A - \Omega_S)w, \\
 \zeta \dot{P} &= -u_b + \frac{\gamma \Omega_S w}{\beta},
 \end{aligned}
 \tag{7.47}$$

where

$$\Omega_j = \frac{c_j}{\nu t_{oc}},
 \tag{7.48}$$

and the parameter ρ in (3.51) and (3.55) is now defined explicitly as

$$\rho = \frac{c_P}{c_S} \sim 1.7 \times 10^{-3},
 \tag{7.49}$$

about half the previously used value; thus also $\gamma \sim 0.04$. To these we must also add the dimensionless

$$\dot{L}_- = \frac{\delta_2}{2\nu} (\Omega_- - \Omega_+) w,
 \tag{7.50}$$

where we have scaled L_- with its present day value L_-^0 . Since $\nu t_{oc} \approx 0.19$ mM, estimates of Ω_j are

$$\Omega_Q \approx 3.05, \quad \Omega_A \approx 4.1, \quad \Omega_S \approx 4, \quad \Omega_- \approx 1.2, \quad \Omega_+ \approx 2.2.
 \tag{7.51}$$

Our earlier estimate of $\Omega_Q = 2$ is regained by having ν one and a half times larger.

Because L_- is approximately constant, we can take the definition of u_p as before. Now letting δ_1, δ_2 be small and taking the limits $\varepsilon, \zeta \rightarrow 0$, we derive the approximate equations

$$\begin{aligned} \eta \dot{Q} &= 2 - \Omega_Q w, \\ \nu \dot{S} &= (1 - \gamma)\Omega_S w - (1 - \Sigma + S), \end{aligned} \tag{7.52}$$

as in (3.63).

Consulting (7.45), we see that presently $\Omega_- < \Omega_+$: weathering of pyrite and gypsum is less than that of enstatite and feldspar. We presume (because of (7.50)) that this was not so in the past, which leads us to suppose that in general the weathering coefficients Ω_j are functions of I . During glacial periods, the former shelf carbonate rocks are exposed, and we might expect r_C to increase; in addition, the advance of the ice over these sediments might enhance the solute flux via the increased erosion which occurs. Table 8 shows that typical subglacially derived runoff delivers slightly lower fluxes than subaerial rivers. Of relevance to the change of carbonate is the aggregated concentration c_S . For rivers this is 0.58 mM, while for glacial streams it is 0.45 mM. From (7.52), we see that a change in the value of Ω_S cannot lead to a rapid decline in S , which is what is needed to elevate p_{CO_2} . Ω_S would have to become negative and large, which is only possible if the pyrite reduction rate r_F increases enormously. The seemingly more likely possibility of increased carbonate weathering actually increases Ω_S , leading to an increase of carbonate and lower p_{CO_2} . We return to this idea later.

The rise of CO_2 from 180 to 280 ppmv at the end of the recent ice ages corresponds to a change of $\Delta \ln p = 0.44$. Inspecting (5.12) and using the numerical values of the parameters in Table 5, we see that (if we take $\Delta I = -1$), 0.16 of this is due to ice albedo, and the remainder must be due to rapid change of S . The change required is $\Delta \ln S = 0.39$, corresponding to a drop by a factor 0.68, or dimensionally a change from 0.36 mM to the present 0.24 mM. Thus we are not seeking a large change in S . However, the only way in which this change can occur rapidly, in terms of our model as represented in (7.52), is if the parameter ν is small. More specifically, we see from (3.55) and (3.52) that the dimensional time scale t_S over which S changes is given by

$$t_S = \frac{2}{k_4 L_-}, \tag{7.53}$$

and is presently about 54 ka, using the value of k_4 in Table 2.

Of course our estimate of these rate constants was partially based on an assumption that the ocean concentrations were in an approximate steady state; which is evidently not the case, as discussed above. However, in order for ν to be sufficiently small to accommodate a rapid change of S , we would need an increase of k_4 of around 20. On the other hand, the scales for S (and Q) seem appropriate, which would suggest that we compensate by increasing the volcanic output ν by a similar amount, and this seems even less likely.

It seems we are forced to conclude that unless the ice-albedo effect is much larger than seems plausible, rapid post-glacial change of atmospheric CO_2 must be due to some other effect which has yet to be considered in the model. There are two which

spring to mind. Firstly, terrestrial biomass provides a major sink for CO₂, and of course it varies rapidly in response to ice cover. However, we might suppose that warmer temperatures cause larger terrestrial biomass and thus increased removal of CO₂ from the atmosphere, which would appear to work in the wrong direction. Secondly, the melt-water from the melting ice sheets is relatively fresh and thus provides a buoyant, less salty surface layer on the world's ocean, and it is this which is in equilibrium with the atmosphere. Thus in principle we might cause a rapid change in CO₂ simply by reducing the carbonate ion of this surface layer, or equivalently by increasing the negative conservative ion concentration. The time scale for ocean mixing is about a thousand years, and so it seems that the freshening of the mixed layer is unlikely to provide a solution, unless the freshening can turn off the formation of deep water, as suggested by [Ganopolski and Rahmstorf \(2001\)](#) in their theory of Dansgaard–Oeschger events.

7.3 Bioproduction

Although examination of both ocean mixing and terrestrial biomass warrant further study, there is another effect which has the possibility of allowing the sudden drop in carbonate that we seek. The clue lies in the equation for P uptake, because the response time t_P of oceanic phosphorus given in (3.61) is of the order of the termination time. In fact with the adjusted value of ρ in (7.49), we have $t_P \sim 12$ ka.

Now we consider the effect of the parameter $b' = b_3 \Delta T > 0$, defined in (3.55), in (3.54). The equations for P , P_B and S (with $\varepsilon, \delta_1, \delta_2 \rightarrow 0$) are, from (7.47), (3.53) and (3.54),

$$\begin{aligned} \zeta \dot{P} &= - \left(P e^{b'\theta} - 1 \right) P_B + \frac{\gamma \Omega_S w}{\beta}, \\ \dot{P}_B &= \frac{\beta}{2\gamma} \left(P e^{b'\theta} - 1 \right) P_B, \end{aligned} \tag{7.54}$$

$$\nu \dot{S} = -\beta \left(P e^{b'\theta} - 1 \right) P_B - (1 - \Sigma) - S + \Omega_S w. \tag{7.55}$$

Recall our present estimates (with the adjusted value of ρ)

$$\begin{aligned} \zeta \sim 0.12, \quad b' \sim 0.9, \quad \gamma \sim 0.04, \quad \beta \sim 1.3, \\ \nu \sim 0.54, \quad \Sigma \sim 0.21, \quad \Omega_S \sim 4. \end{aligned} \tag{7.56}$$

From these we have

$$\frac{\beta}{2\gamma} \sim 16.3, \quad \frac{\gamma \Omega_S}{\beta} \sim 0.12. \tag{7.57}$$

Thus, approximately, we have during termination

$$\dot{P}_B \approx \frac{\beta}{2\gamma} u_b, \quad \zeta \dot{P} \approx -u_b, \quad \nu \dot{S} \approx -\beta u_b, \tag{7.58}$$

where

$$u_b = \left(P e^{b'\theta} - 1 \right) P_B. \tag{7.59}$$

From these it follows that P satisfies

$$\dot{P} \approx \frac{\beta}{2\gamma} \left(P e^{b'\theta} - 1 \right) (P - C), \tag{7.60}$$

where C is constant, and thus P hunts its equilibrium $e^{-b'\theta}$ on a termination time scale

$$t_T = \frac{2\gamma}{\beta B} = \frac{1}{k_{-3}} \sim 7,000 \text{ year}. \tag{7.61}$$

As P and thus P_B adjust to their new postglacial equilibrium, S follows passively. According to (7.58), the change in S during termination is

$$\Delta S \approx \frac{\beta \zeta}{\nu} \Delta(e^{-b'\theta}) \approx -\frac{\beta \zeta b'}{\nu} \Delta\theta, \tag{7.62}$$

and taking $\Delta\theta = 1$, this is $\Delta S \approx -0.26$. As discussed above, we must have $\Delta S \approx -0.44$ (corresponding to the drop from 0.36 to 0.24 mM), and this can be effected if $b' = 1.5$, corresponding to a doubling of bioproductivity every 6 K, rather than the 10 K we assumed earlier.

8 Numerical results

Preamble

Having apparently assembled the ingredients to reproduce the observational data, we now begin the task of aligning the model with the data. On the assumption that the basic behaviour of the solutions has the right structure, this is a matter of adjusting some of the loosely constrained parameters in order to provide a cosmetically pleasing fit to the observations.

There is, however, yet another obstacle to overcome. Although thermally activated biomass production can produce the sharp rising limb of the CO₂ curve, the descending limb wanders away from that of temperature. The reason can be understood in terms of the nullcline of the carbonate equation (7.52), and the remedy consists of wrestling this nullcline round so that S does not follow the ice volume down during glacials. This is effected by having the carbonate weathering rate being increased when the continental shelves are exposed, as already suggested in Sect. 7. With this adjustment, it is not too difficult to find reasonable parameter values that provide a satisfactory fit to the data.

Finally, we add a time-dependent forcing resembling Milanković variation. As we might expect, this produces relatively small, higher frequency jitters on top of the basic oscillation, causing its period and amplitude to vary irregularly.

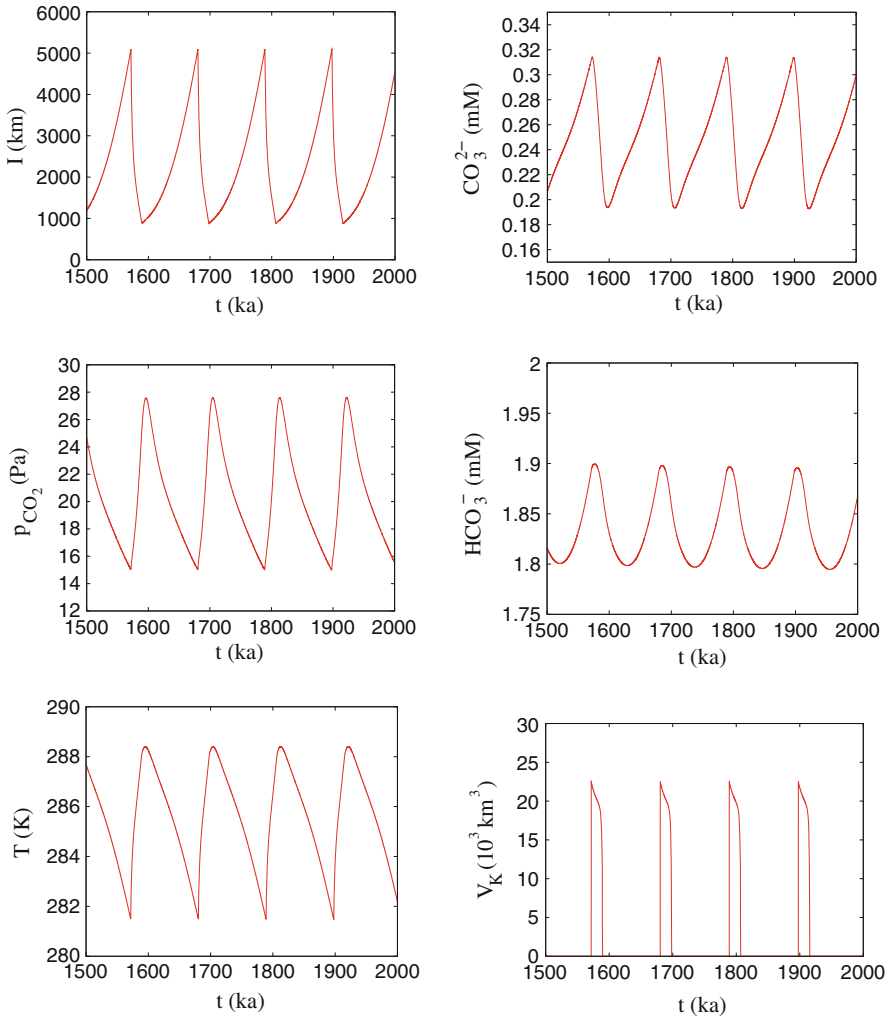


Fig. 14 Reading each row from the *left*, and from the *top down*, the figure shows plots of I , S , p , Q , T and lake volume V_K , all in the indicated dimensional units, in terms of time t measured in ka, using the ‘used’ parameters in Table 9

8.1 Numerical method

In our numerical model, we solve the four equations in (7.47), together with the fourth, sixth and seventh equations in (5.1), and also equation (6.6), using the subsidiary relations defined in (5.3). We use a fourth order Runge Kutta method, and the code is written in Fortran. In the simulations shown in Fig. 14, we have used a different runoff function defined by

$$r = \exp[\exp\{10(v - 1)\}], \tag{8.1}$$

not for any reason other than a mistaken concern that the function in (6.11) might be a cause of numerical instability. In fact, the primary cause of numerical breakdown appears to be the use of the maximum and Heaviside functions in (4.41), whose lack of smoothness can be expected to cause problems for the fourth order Runge Kutta method. In practice, we use approximating functions

$$\begin{aligned}
 f_{\text{Heav}}(z) &= \frac{1}{2} \left\{ 1 + \tanh \left(\frac{z}{d_1} \right) \right\}, \\
 f_{\text{max}}(x, y) &= \frac{1}{2} \left[x + y + d_2 \log \left\{ 2 \cosh \left(\frac{x - y}{d_2} \right) \right\} \right],
 \end{aligned}
 \tag{8.2}$$

where the values of the positive parameters d_1 and d_2 should be small; in practice, values of $d_1 = d_2 = 0.25$ are needed for numerical stability. The various other functions f , Ξ , α are as defined earlier.

The parameters used in obtaining Fig. 14 are given in Table 9. It is worth outlining our approach to obtaining the graphs in this figure, as we now enter the murky realm of curve-fitting. We begin with the default parameters as defined in the earlier tables. The ice accumulation rate a_i is based on an Antarctic value, with little particular reason; the same applies to the melt rate m_i , but as discussed earlier, the value of the melt rate when the ice is retreating must be larger in order that the termination can be rapid. Experimentation with increasing values indicates that potentially the value $m_- = 6 \text{ m year}^{-1}$ provides a useful value about which other experiments can be conducted. For this value, we find that glacial terminations do occur rapidly, and the period is of the right order, but the carbonate and bicarbonate concentrations are too high.

Table 9 Default values of the parameters as given in Tables 2, 3, 4 and 6 and equation (7.46), see also equation (8.4), together with the values used in producing Fig. 14

Parameter	Default	Used
B (year^{-1})	10^{-5}	0.3×10^{-5}
b_3 (K^{-1})	0.069	0.15
c_Q (mM)	0.58	0.72
c_S (mM)	0.76	0.44
d_i (m)	4	3
h_0 (m)	1,200	400
k_4 ($\text{M}^{-1} \text{ year}^{-1}$)	2.1×10^{-3}	1.8×10^{-3}
m_- (m year^{-1})	2	7
p_0 (Pa)	28	40
T_0 (K)	288	291
θ_I (K)	5	3
κ_S	0	0.5

There now follows a needle in haystack search for an appropriate parameter set. In conducting these numerical experiments, we have found that the nature of the oscillatory solutions which are obtained is quite sensitive to the precise values of the parameters. Since we have a huge number of reasonably adjustable parameters, a methodical search requires more than the effort exhibited here; however, as with all curve-fitting exercises, the effort becomes wasteful if pursued to extremes. On the other hand, scientists are loathe to believe any theoretical exercise unless it fits observations very closely.

In our experiments, we have aimed to fit the rapid terminations and the associated rapid rise in p_{CO_2} from ~ 18 to ~ 28 Pa, as well as the general levels of maximum ice extent, present CO_3^{2-} and HCO_3^- levels, temperature fluctuation, and 100 ka period. This is of course an awkward and perhaps fruitless problem. In order to fit eight different categories of observation, we may expect to adjust at least eight different parameters. In fact we have adjusted twelve, largely by iteration and using our understanding of their effect on the likely behaviour of the model. We now trace the particular route to the choice in Table 9.

Increased m_- enables the rapid terminations, but to get them as short as 10 ka is difficult. To this end we reduced the calcium carbonate burial rate, which has the effect of reducing the dimensionless time constant ω , but in reality this is of little importance.

8.2 Enhanced carbonate weathering

The principal problem is that although there is a jump in CO_2 at termination, it is not large enough; worse, the CO_2 fluctuates during the ice age and does not follow the ice volume. Consideration of the $I-S$ phase plane, and specifically the S nullcline of (7.52)₂, shows (using (5.12)₃) that during an ice age S migrates towards a decreasing function of I . More specifically, this is

$$\left\{ \frac{(1 - \gamma)\Omega_S}{1 - \Sigma + S} \right\}^{(1-\lambda b)} \left(\frac{Q^2}{S} \right)^{(\mu+\lambda)} = \exp[\kappa(1 + \mu b)I]. \tag{8.3}$$

Since p is inversely proportional to S , and we need p to decline with I , we see that we need S to increase uniformly as I decreases, and this is disabled by the relatively rapid approach of S towards the S nullcline, which causes S first to rise and then fall.

One way round this is to increase the carbonate time scale $t_S = \frac{2}{k_4 L_-}$, which implies reducing k_4 . This does not work effectively, and moreover has the consequent negative result that the carbonate and bicarbonate scales S_0 and Q_0 are increased. Since, from (7.52), Q at equilibrium is a decreasing function of Ω_Q and thus c_Q , while S at equilibrium is an increasing function of c_S , this suggests that the size of Q and S can be adjusted by altering these concentrations.

Nevertheless, the p profile refuses to fall into line. We can increase the jump in p at termination by increasing the biomass production rate dependence on temperature b_3 , as discussed following (7.54), but in order to get a reasonable S (and thus p) profile, we really need to shift the S nullcline so that S does not decrease with I . The way we propose to do this is to introduce an ice volume dependence of the weathering rate

Ω_S , so that in particular

$$\Omega_S = \Omega_S^0 \exp(\kappa_S I). \tag{8.4}$$

What would cause such an amplification? We already know that weathering rates must have varied over an ice age, so the proposition of (8.4) is not all that controversial. The principal difference between glacials and interglacials is that during interglacials, the continental shelves are inundated, and shallow marine carbonate burial ensues. During a glacial period, sea level retreat exposes these soft carbonates, and we might expect that carbonate erosion rates would increase. Consulting (7.45), we see that increased carbonate runoff r_C increases c_A and c_S , and hence Ω_A and Ω_S , of which only the latter is important. The choice of $\kappa_S = 0.5$ in Table 9 represents an increase of carbonate weathering by a factor of 1.65 at glacial maximum.

The inclusion of $\kappa_S > 0$ has an immediate effect: the CO_2 profile becomes as required. Because of this immediate success, we have not explored the effect of changing ice volume dependence of other weathering coefficients, or even of trying different values of κ_S .

Essentially, the choice of non-zero b_3 and κ_S provide the key ingredients which allow both a rapid jump in CO_2 and also the slow decline during the glacial period. Without both of these effects, it is difficult in this model to find solutions resembling the data.

Having found the necessary ingredients to produce the shape, it remains to adjust the scale: the range of p from 18 to 28 Pa; the range of T from 283 to 288 K; the post-glacial values of $S \sim 0.24$ mM and $Q \sim 1.7$ mM; the maximum ice extent of $I \sim 4,000$ km; and the period of ~ 100 ka. Finding these values is largely a cosmetic exercise, and can be done by adjusting the loosely constrained parameters p_0 , T_0 , θ_I and d_i , and also the input concentrations c_Q and c_S . Ideally, we would adjust these to produce a more precise fit, but that is essentially an academic exercise with no scientific purpose.

8.3 Milanković variations

Finally we turn to a consideration of the possible effects of Milanković fluctuations. We will not deal in detail with this, because a whole new raft of issues confront us: we will defer a detailed discussion to future work. However, we can outline what these issues are.

In our model, we represent Milanković variation through its effect on the Arctic Ocean snowline elevation, which translates to the dimensionless parameter H . Time-dependent fluctuations are represented by the function q_M in (5.8), which we take to be given by the (dimensionless) function

$$q_M = a_1 \cos \omega_1 t + a_2 \cos \omega_2 t, \tag{8.5}$$

where the dimensionless frequencies ω_i are given by

$$\omega_i = \frac{2\pi}{BP_i}, \tag{8.6}$$

and where P_i are the dimensional periods of the forcing (we take $P_1 = 23$ ka and $P_2 = 41$ ka). This causes the S nullcline in Fig. 8 to oscillate back and forth relatively rapidly, and the effect of this is to cause fairly small amplitude higher frequency oscillations in the variables, together with fluctuations in the peak values. On the other hand, the data in Fig. 2 suggests that the peaks are relatively uniform, and we can accommodate this by modifying the definition of the normal ice melting rate m_i , and thus the parameter α_+ . The reason for doing this is that as the ice sheet increases in extent, it migrates south, where the summer melting will increase. We model this by taking α_+ as an increasing function of I , and in our simulations, we choose

$$\alpha_+ = \alpha_+^0 \exp \left[e^{\alpha_M(I-1)} - 1 \right] \tag{8.7}$$

in (6.11). The point is that, from (6.12), proglacial lakes form and the ice age terminates when

$$\Xi\alpha_+(I) \approx (I + k^*H)^2\alpha_+(I) \approx \frac{1}{M^*} \tag{8.8}$$

(see (6.9)), and if α_+ increases abruptly near $I = 1$, then termination will occur near this value, providing $M^* < 1$. Since with the default parameters of Fig. 14, $M^* = 0.922$, we have reduced l_p to 2,000 km to enable this. We might equally have increased the runoff scale R_K^0 .

Figure 15 shows the result of a computation which shows these general effects, and this figure can be directly compared to Fig. 2. We see variability in amplitude and period, as well as occasionally interrupted terminations (e.g., at age 95 ka). On the

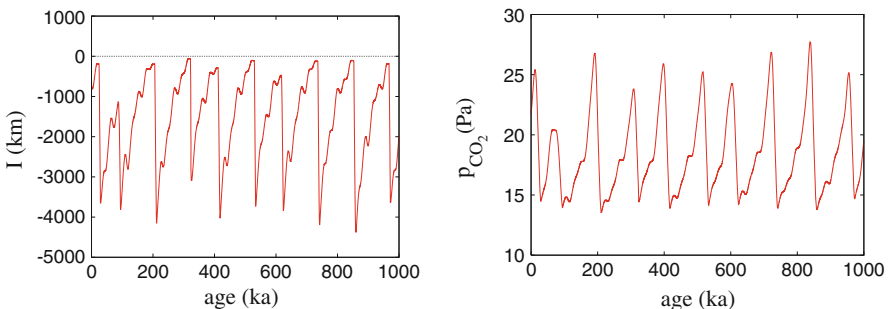


Fig. 15 Solution for ice extent (plotted as $-I$) and CO_2 as functions of age (with present day being at $t = 2,000$ ka); the same parameters as in Fig. 14 are used, but with the pseudo-Milanković forcing q_M (see (5.8)) given by (8.5), with $a_1 = 0.8$, $P_1 = 23$ ka, $a_2 = 0.5$, $P_2 = 41$ ka, and the values of $\alpha_M = 3$ (see (8.7)) and $l_p = 2 \times 10^6$ m

negative side, the fluctuations are relatively small, a consequence of their relatively high frequency.

Of course, Fig. 15 has none of the high frequency variability indicated by the observations, and this is perhaps unsurprising, as there is apparently no high frequency oscillation mechanism in our model. Some of the high frequency components of the data may be associated with the occurrence of Dansgaard–Oeschger events, whose explanation may lie in altered patterns of North Atlantic circulation (Ganopolski and Rahmstorf 2001) due to variation of freshwater input. Evatt et al. (2006) have suggested that the source of such freshwater might be subglacial lake floods, but equally we might suppose proglacial lake floods. A nice way of having an aborted termination is to build proglacial lakes which then suddenly drain, and this seems to be an avenue worth exploring in the future. Indeed, it seems that if disturbance of the ocean circulation by fresh water explains millennial climate shifts, then the only possible mechanism is through massive floods from huge melting events, with consequent sea level rise, and such variations in sea level have been suggested by Siddall et al. (2003).

9 Discussion

The model that we have eventually derived and solved is given from (7.47), (5.1)_{4,6,7}, (6.6) and (5.3) by the dimensionless set

$$\begin{aligned}
 \varepsilon \dot{p} &= 1 - \Lambda(p - p_s) - \Omega_A w, \\
 \eta \dot{Q} &= 2\Lambda(p - p_s) + (2\Omega_A - \Omega_Q)w, \\
 \nu \dot{S} &= -\beta u_b - u_p - \Lambda(p - p_s) - (\Omega_A - \Omega_S)w, \\
 \zeta \dot{P} &= -u_b + \frac{\gamma \Omega_S w}{\beta}, \\
 \dot{N} &= \beta u_b + u_p - N, \\
 \dot{P}_B &= \frac{\beta u_b}{2\gamma} - P_B, \\
 \omega \dot{I} &= f(I, H, \alpha), \\
 \delta \dot{v} &= M^* \Xi(I, H)\alpha(v) - r(v),
 \end{aligned} \tag{9.1}$$

where

$$\begin{aligned}
 \theta &= \lambda \ln p - \kappa I, \\
 p_s &= \frac{Q^2 e^{b\theta}}{S}, \\
 u_b &= (P e^{b'\theta} - 1) P_B, \\
 u_p &= S(1 + \delta_1 Q + \delta_2 S) - \Sigma, \\
 w &= p^\mu e^\theta,
 \end{aligned} \tag{9.2}$$

and we have painted a clear picture of the solutions. The ice sheet/proglacial lake sub-model for I and v has spontaneous periodic oscillations, and it is these which cause the succession of ice ages. Carbon is a passive player, and is controlled by the enslavement of the ocean carbonate ion to the ice volume. The apparent following by CO_2 of the temperature signal is due to thermally activated growth of oceanic biomass, together with enhanced carbonate weathering of exposed continental shelves. At least, in the model. Whether these conclusions apply in reality remains to be seen.

Our vision of the paleoclimate, as interpreted within the confines of the admittedly simple model we have proposed, is as follows. We hypothesise that the long term climate of the planet is controlled by ice cover and by CO_2 , which itself is determined by bicarbonate Q and carbonate ions S in the ocean, as given in (5.12). In the model we have presented, ice cover itself depends hysteretically on H , and thus temperature, and thus ocean carbon. From (5.12), we have

$$\theta = \frac{\lambda}{\mu + \lambda} \ln w - \frac{\mu\kappa I}{\mu + \lambda}, \tag{9.3}$$

and the weathering term w is determined, on a time scale of ~ 1 Ma, by (7.52), i.e.,

$$w = \frac{2}{\Omega_Q}. \tag{9.4}$$

In the absence of ice, the planet cools in the Eocene by increase of Ω_Q . Consulting (7.38) and (7.48), we see that this implies increasing precipitation and thus runoff, decreasing volcanic production of CO_2 , or else increasing weathering, particularly of silicates (according to (7.34) and (7.45)); or, of course, all three.

As the planet cools, H decreases, and first Antarctica, then Greenland, then the Laurentide ice sheets grow hysteretically. Antarctica and Greenland are both bounded by ocean, but the Laurentide is bounded to the south by land. Both the land and the southerly latitude allow melting to form proglacial lakes, whose presence, we suppose, hugely enhances the wastage rates, and allows the ice sheet to wither before it can reach its desired steady state. One might wonder, why does the disappearing ice sheet jump across the Nares Strait but not cause the Greenland Ice Sheet to vanish also, since it is at much lower latitude than Ellesmere Island? The answer to this is presumably that the collapse of the Labrador Sea ice shelf/sea ice allows for precipitation over Greenland to be significantly higher than when the Laurentide is present, and so the ice sheet is maintained.

As the planet cools, the benthic $\delta^{18}\text{O}$ signal changes from a 40 ka periodicity to an approximate 100 ka one, some 1 Ma ago. It is fairly easy to see how this should come about. When an ice sheet is stable, as we suppose the Antarctic and Greenland ice sheets to be, then modulation of them by a quasi-periodic input will cause a similar quasi-periodic output, as in Fig. 9. However, if the Laurentide Ice Sheet is intrinsically oscillatory, then the modulations will cause wobbles and fluctuations, as in Fig. 15.

Much has been made of the apparent lead of CO_2 by Antarctic T at glacial terminations, with a response interval of several hundred years. Our main view is that worry about such details is inappropriate if the basic oscillation mechanism is not

understood, but having said that, it is also the case in our model results. For example, in Fig. 15, the glacial maximum at age 211,670 yr (the first we looked at) is followed by a CO₂ minimum at age 211,300 yr, an interval of 370 years. This detail is not of significance, however, and perhaps not even of relevance. Recently, [Shakun et al. \(2012\)](#) have suggested that CO₂ trails global average temperature, and that the mismatch between Antarctic and global temperatures is due to ocean transport between the hemispheres—which is of course not considered within the present model.

10 Conclusions

We have sequentially developed the conceptually simplest model we can imagine in order to try and explain the observations of ice volume and CO₂ during the Pleistocene ice ages. Our ideas, derived with some degree of effort, are nevertheless neither revolutionary nor even novel. Almost all the ingredients have been mooted before in some form. The novelty of our approach is that we avoid out-and-out simulation, and have relentlessly endeavoured to understand the model behaviour, and use this understanding to introduce additional mechanisms when necessary to explain the observations. This sort of approach is unconventional, but, we would argue, of great intrinsic merit.

The model involves a description of ice-albedo feedback, the CO₂ greenhouse effect, carbon buffering in the ocean, and as a consequence, also P-limited biomass production. In seeking mechanisms to account for rapid CO₂ rise and rapid terminations, we have been led to propose that enhanced wastage by proglacial lakes and the temperature dependence of oceanic biomass growth are essential ingredients in the model if it is to explain the behaviour which is seen. This does not necessarily mean that these effects are as important in reality as we contend they must be in the model. Many other mechanisms and processes have been ignored by us. For example, we have been led to hypothesise a reasonably strong dependence of ocean biomass growth on temperature, because, within this model, there seems little alternative mechanism to produce rapid postglacial CO₂ rise. This does not in any way preclude other putative mechanisms, but we do not know what they might be.

We emphasise that we have at every stage introduced new complications because the data has driven us to do so. If these mechanisms are incorrect, then others must take their place. Despite this, there are many constituent parts of the Earth system which may be of fundamental importance. An obvious example is that of the dynamics of the oceans, and ocean temperature and salinity; these were important constituents of [Saltzman's \(2002\)](#) investigations. Another is the rôle of terrestrial biomass, which must be strongly affected during ice ages, and which plays a central part in the dynamics of atmospheric carbon. We do not deny the importance of these, simply we have not yet been led to include them; we may need to do this in the future.

Apart from mechanism, the other obvious shortcoming in a simple model like this is the lack of spatial variability, both in the vertical (mixed layer versus deep ocean) and the horizontal (poleward energy transport in the energy balance model). It is not obvious on long time scales whether either of these will be significant, but they are clearly a matter for investigation.

Despite these reservations, the effort we have expended leads us to promote our vision of planetary paleoclimate robustly. Models must explain data, but equally, data is provided by systems which obey physical laws, which are described by models. It is not easy to derive models which will reasonably produce the data of Figs. 1 and 2. Within the limited confines of our box structure, we consider that the key components of proglacial lake formation, thermally activated biomass production and enhanced carbonate weathering may also be essentially important in more detailed models.

Acknowledgments A.C.F. acknowledges the support of the Mathematics Applications Consortium for Science and Industry (<http://www.macci.ul.ie>) funded by the Science Foundation Ireland mathematics initiative grant 06/MI/005.

References

- Archer, D., Khesghi, H., Maier-Reimer, E.: Multiple timescales for neutralization of fossil fuel CO₂. *Geophys. Res. Lett.* **24**, 405–408 (1997)
- Berger, W.H.: Increase of carbon dioxide in the atmosphere during deglaciation: the coral reef hypothesis. *Naturwissenschaften* **69**, 87–88 (1982)
- Berger, A.: Milankovitch theory and climate. *Revs. Geophys.* **26**, 624–657 (1988)
- Bigg, G.: *The Oceans and Climate*, 2nd edn. CUP, Cambridge (2003)
- Boulton, G.S., Hagdorn, M., Maillot, P.B., Zatzepin, S.: Drainage beneath ice sheets: groundwater–channel coupling, and the origin of esker systems from former ice sheets. *Quat. Sci. Rev.* **28**, 621–638 (2009)
- Broecker, W.S., Peng, T.-H.: *Tracers in the Sea*. Eldigio Press, New York (1982)
- Budyko, M.I.: The effect of solar radiation variations on the climate of the Earth. *Tellus* **21**, 611–619 (1969)
- Caldeira, K.: Enhanced Cenozoic chemical weathering and the subduction of pelagic carbonate. *Nature* **357**, 578–581 (1992)
- Cheng, H., Edwards, R.L., Broecker, W.S., Denton, G.H., Kong, X., Wang, Y., Zhang, R., Wang, X.: Ice age terminations. *Science* **326**, 248–252 (2009)
- Croll, J.: On the physical cause of the change of climate during geological epochs. *Phil. Mag.* **28**(4), 121–137 (1864)
- Croll, J.: *Climate and Time in Their Geological Relations: A Theory of Secular Changes of the Earth's Climate*. Daldy, Isbister, London (1875)
- Cuffey, K., Paterson, W.S.B.: *The Physics of Glaciers*, 4th edn. Butterworth-Heinemann, Oxford (2010)
- Emerson, S.R., Hedges, J.I.: *Chemical Oceanography and the Marine Carbon Cycle*. CUP, Cambridge (2008)
- Evatt, G., Fowler, A.C., Clark, C.D., Hulton, N.: Subglacial floods beneath ice sheets. *Phil. Trans. R. Soc.* **364**, 1769–1794 (2006)
- Foster, G.L., Vance, D.: Negligible glacial-interglacial variation in continental weathering rates. *Nature* **444**, 918–921 (2006)
- Fowler, A.C.: *Mathematical Geoscience*. Springer, London (2011)
- Ganopolski, A., Rahmstorf, S.: Rapid changes of glacial climate simulated in a coupled climate model. *Nature* **409**, 153–158 (2001)
- Ghil, M., Le Treut, H.: A climate model with cryodynamics and geodynamics. *J. Geophys. Res.* **86**, 5262–5270 (1981)
- Goldbeter, A.: *Biochemical Oscillations and Cellular Rhythms*. CUP, Cambridge (1996)
- Hays, J.D., Imbrie, J., Shackleton, N.J.: Variations in the Earth's orbit: pacemaker of the ice ages. *Science* **194**, 1121–1132 (1976)
- Hodson, A.: Phosphorus in glacial meltwaters. In: Knight, P.G. (ed.) *Glacier Science and Environmental Change*, pp. 81–82. Blackwell, Oxford (2006)
- Houghton, J.T.: *Global Warming: The Complete Briefing*, 4th edn. CUP, Cambridge (2009)
- Huybers, P.: Early Pleistocene glacial cycles and the integrated summer insolation forcing. *Science* **313**, 508–511 (2006)
- Jahnke, R.A.: The phosphorus cycle. In: Butcher, S.S., Charlson, R.J., Orians, G.H., Wolfe, G.V. (eds.) *Global Biogeochemical Cycles*, pp. 301–315. Academic Press, London (1992)

- Källén, E., Crafoord, C., Ghil, M.: Free oscillations in a climate model with ice-sheet dynamics. *J. Atmos. Sci.* **36**, 2292–2303 (1979)
- Kawamura, K., Parrenin, F., Lisiecki, L., Uemura, R., Vimeux, F., Severinghaus, J.P., Hutterli, M.A., Nakazawa, T., Aoki, S., Jouzel, J., Raymo, M.E., Matsumoto, K.H., Nakata, Motoyama, H., Fujita, S., Goto-Azuma, K., Fujii, Y., Watanabe, O.: Northern Hemisphere forcing of climatic cycles in Antarctica over the past 360,000 years. *Nature* **448**, 912–916 (2007)
- Krauskopf, K.B., Bird D.K.: *Introduction to Geochemistry*, 3rd edn. McGraw-Hill, New York (1995)
- Laskar, J., Robutel, P., Joutel, F., Gastineau, M., Correia, A.C.M., Levrard, B.: A long-term numerical solution for the insolation quantities of the Earth. *Astron. Astrophys.* **428**, 261–285 (2004)
- Le Treut, H., Ghil, M.: Orbital forcing, climatic interactions, and glaciation cycles. *J. Geophys. Res.* **88**, 5167–5190 (1983)
- Leverington, D.W., Mann, J.D., Teller, J.T.: Changes in the bathymetry and volume of Glacial Lake Agassiz between 11,000 and 9,300 ^{14}C yr b.p. *Quat. Res.* **54**, 174–181 (2000)
- Lisiecki, L.E., Raymo, M.E.: A Pliocene-Pleistocene stack of 57 globally distributed benthic $\delta^{18}\text{O}$ records. *Paleoceanography* **20**, PA1003 (2005). doi:[10.1029/2004PA001071](https://doi.org/10.1029/2004PA001071)
- Maasch, K.A., Saltzman, B.: A low-order dynamical model of global climatic variability over the full Pleistocene. *J. Geophys. Res.* **95**, 1955–1963 (1990)
- MacAyeal, D.R.: A catastrophe model of the paleoclimate. *J. Glaciol.* **24**, 245–257 (1979)
- Mackenzie, F.T., Lerman, A., Andersson, A.J.: Past and present of sediment and carbon biogeochemical cycling models. *Biogeosciences* **1**, 11–32 (2004)
- Milanković, M.: Canon of insolation and the ice-age problem. Translated from German edition of 1941. Agency for Textbooks, Belgrade (1998)
- Munhoven, G.: Glacial-interglacial changes of continental weathering: estimates of the related CO_2 and HCO_3^- flux variations and their uncertainties. *Glob. Planet. Change* **33**, 155–176 (2002)
- Murton, J.B., Bateman, M.D., Dallimore, S.R., Teller, J.T., Yang, Z.: Identification of Younger Dryas outburst flood path from Lake Agassiz to the Arctic Ocean. *Nature* **464**, 740–743 (2010)
- Oerlemans, J.: Model experiments on the 100,000-yr glacial cycle. *Nature* **287**, 430–432 (1980)
- Oerlemans, J.: Some basic experiments with a vertically-integrated ice sheet model. *Tellus* **33**, 1–11 (1981)
- Pagani, M., Huber, M., Liu, Z., Bohaty, S.M., Henderiks, J., Sijp, W., Krishnan, S., DeConto, R.M.: The role of carbon dioxide during the onset of Antarctic glaciation. *Science* **334**, 1261–1264 (2011)
- Petit, J.R., Jouzel, J., Raynaud, D., Barkov, N.I., Barnola, J.-M., Basile, I., Bender, M., Chappellaz, J., Davis, M., Delaygue, G., Delmotte, M., Kotlyakov, V.M., Legrand, M., Lipenkov, V.Y., Lorius, C., Pépin, L., Ritz, C., Saltzman, E., Stevenard, M.: Climate and atmospheric history of the past 420,000 years from the Vostok ice core. *Antarctica. Nat.* **399**, 429–436 (1999)
- Parrenin, F., Paillard, D.: Amplitude and phase of glacial cycles from a conceptual model. *Earth Planet. Sci. Lett.* **214**, 243–250 (2003)
- Pollard, D.: A simple ice sheet model yields realistic 100 kyr glacial cycles. *Nature* **296**, 334–338 (1982)
- Pollard, D., DeConto, R.M.: Hysteresis in Cenozoic Antarctic ice-sheet variations. *Global Planet. Change* **45**, 9–21 (2005)
- Raymo, M.E., Lisiecki, L.E., Nisancioglu, K.H.: Plio-Pleistocene ice volume, Antarctic climate, and the global $\delta^{18}\text{O}$ record. *Science* **313**, 492–495 (2006)
- Ridgwell, A.J., Kennedy, M.J., Caldeira, K.: Carbonate deposition, climate stability, and Neoproterozoic ice ages. *Science* **302**, 859–862 (2003)
- Ridgwell, A., Zeebe, R.E.: The role of the global carbonate cycle in the regulation and evolution of the Earth system. *Earth Planet. Sci. Lett.* **234**, 299–315 (2005)
- Saltzman, B.: *Dynamical Paleoclimatology: Generalized Theory of Global Climate Change*. Academic Press, San Diego (2002)
- Saltzman, B., Maasch, K.A.: Carbon cycle instability as a cause of the late Pleistocene ice age oscillations: modeling the asymmetric response. *Global Biogeochem. Cycles* **2**, 177–185 (1988)
- Saltzman, B., Maasch, K.A.: A first-order global model of late Cenozoic climatic change. II. Further analysis based on a simplification of CO_2 dynamics. *Clim. Dyn.* **5**, 201–210 (1991)
- Saltzman, B., Hansen, A.R., Maasch, K.A.: The late Quaternary glaciations as the response of a three-component feedback system to Earth–orbital forcing. *J. Atmos. Sci.* **41**, 3380–3389 (1984)
- Sellers, W.D.: A climate model based on the energy balance of the earth-atmosphere system. *J. Appl. Meteorol.* **8**, 392–400 (1969)

- Shakun, J.D., Clark, P.U., He, F., Marcott, S.A., Mix, A.C., Liu, Z., Otto-Bliesner, B., Schmittner, A., Bard, E.: Global warming preceded by increasing carbon dioxide concentrations during the last deglaciation. *Nature* **484**, 49–55 (2012)
- Shreve, R.L.: Esker characteristics in terms of glacier physics, Katahdin esker system, Maine. *Geol. Soc. Amer. Bull.* **96**, 639–646 (1985)
- Siddall, M., Rohling, E.J., Almogi-Labin, A., Hemleben, Ch., Melschner, D., Schmelzer, I., Smeed, D.A.: Sea-level fluctuations during the last glacial cycle. *Nature* **423**, 853–858 (2003)
- Toggweiler, J.R.: Origin of the 100,000-year timescale in Antarctic temperatures and atmospheric CO₂. *Paleoceanogr.* **23**, PA2211 (2008). doi:[10.1029/2006PA001405](https://doi.org/10.1029/2006PA001405)
- Tranter, M.: Glacial chemical weathering, runoff composition and solute fluxes. In: Knight, P.G. (ed.) *Glacier Science and Environmental Change*, pp. 71–75. Blackwell, Oxford (2006)
- Tziperman, E., Raymo, M.E., Huybers, P., Wunsch, C.: Consequences of pacing the Pleistocene 100 kyr ice ages by nonlinear phase locking to Milanković forcing. *Paleoceanogr.* **21**, PA4206 (2006). doi:[10.1029/2005PA001241](https://doi.org/10.1029/2005PA001241)
- Walker, J.C.G., Hays, P.B., Kasting, J.F.: A negative feedback mechanism for the long-term stabilization of Earth's surface temperature. *J. Geophys. Res.* **86**(C10), 9776–9782 (1981)
- Weertman, J.: Milanković solar radiation variations and ice age ice sheet sizes. *Nature* **261**, 17–20 (1976)
- Wingham, D.J., Siegert, M.J., Shepherd, A., Muir, A.S.: Rapid discharge connects Antarctic subglacial lakes. *Nature* **440**, 1033–1037 (2006)
- Wolff, E.W., Fischer, H., Röthlisberger, R.: Glacial terminations as southern warmings without northern control. *Nat. Geosci.* **2**, 206–209 (2009)
- Zeebe, R.E., Westbroek, P.: A simple model for the CaCO₃ saturation state of the ocean: the “Strangelove”, the “Neritan”, and the “Cretan” ocean. *Geochem. Geophys. Geosyst.* **4**, 1104 (2003). doi:[10.1029/2003GC000538](https://doi.org/10.1029/2003GC000538)
- Zeebe, R.E., Wolf-Gladrow, D.: *CO₂ in Seawater: Equilibrium, Kinetics, Isotopes*. Elsevier, Amsterdam (2001)